

A Regularization Strategy for the Two-Dimensional Active Layer Model

Development and Implementation in Delft3D-FM



This research has been possible thanks to the research programme RiverCare, supported by the Dutch Applied and Engineering Sciences (TTW) domain of the Netherlands Organization for Scientific Research (NWO), and which is partly funded by the Ministry of Economic Affairs under grant number P12-14 (Perspective Programme). The research has been partially conducted at the Delft University of Technology under the supervision of **Astrid Blom** and **Ralph Schielen** (appointed also in Rijkswaterstaat) and in Deltares. Part of the funding comes from the Rivers2Morrow program, which is fully funded by the Ministry of Infrastructure and Water Management and its executive organization Rijkswaterstaat. We greatly acknowledge the support of **Matthijs Boersema** in making this project possible.



Rijkswaterstaat
Ministerie van Infrastructuur en Milieu





A Regularization Strategy for the Two-Dimensional Active Layer Model

Development and Implementation in Delft3D-FM

Victor Chavarrias

11203684-006

©Deltares, 2019

Title

A Regularization Strategy for the Two-Dimensional Active Layer Model

Client	Project	Reference	Pages
Rijkswaterstaat Verkeer en Leefomgeving, UTRECHT	Water, 11203684-006	11203684-006-ZWS-0001	70



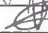

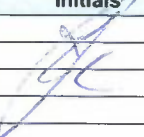
Classification**Keywords**

active layer model, 2D morphodynamics, ill-posedness

Summary

The active layer model used to account for mixed-size sediment morphodynamic processes may be ill-posed under certain circumstances. Well-posedness guarantees the existence of a unique solution continuously depending on the problem data. When a model becomes ill-posed, infinitesimal perturbations to a solution grow infinitely fast. Apart from the fact that this behaviour cannot represent a physical process, numerical simulations of an ill-posed model continue to change as the grid is refined. For this reason, ill-posed models cannot be used as predictive tools. There exists a regularization strategy that guarantees that the one-dimensional active layer model is well-posed. Here we show that the extension of this strategy to two dimensions does not regularize the model. We propose a different regularization strategy that guarantees that the two-dimensional active layer model is well-posed. We implement the two-dimensional regularization strategy in Delft3D-FM and apply it to an idealized case and a field case.

References

Version	Date	Author	Initials	Review	Initials	Approval	Initials
1.0	25-10-2019	Victor Chavarrias		Willem Ottevanger			
2.0	01-11-2019	Victor Chavarrias		Willem Ottevanger		Johan Boon	

Status

final

For the sake of completeness of this document, rather than referring to the paper, Sections 2 and 5 are extracted with little or no modification from the Open Access publication from the same author *Chavarrías et al.* (2019a).

Contents

List of Tables	iii
1 Introduction	1
2 Original Model Equations	3
2.1 Conservation Equations	3
2.1.1 Flow Equations	3
2.1.2 Morphodynamic Equations	4
2.2 Closure Relations	5
3 Regularization Strategy	9
3.1 Modification of the Time Scale of Mixing Processes	9
3.2 Addition of Diffusion to the Active Layer Equation	9
4 Linearization of the System of Equations	11
4.1 Water Mass Conservation	11
4.2 Water Momentum Conservation in x Direction	12
4.3 Water Momentum Conservation in y Direction	13
4.4 Sediment Mass Conservation for the Entire Mixture	14
4.5 Sediment Mass Conservation for each Grain Size in the Active Layer	18
5 Perturbation Analysis	21
5.1 Matrix Formulation	21
5.2 Eigenvalue Problem	23
5.3 Instability, Hyperbolicity, and Ill-Posedness	24
6 Analytical Results	29
6.1 Two Sediment Size Fractions Model	29
6.2 Ill-posedness Test	31
6.3 Effect of Modifying the Time Scale of Mixing Processes in the 2D Model	32
6.4 Effect of Adding Diffusion to the Active Layer Equation in the 2D Model	32
7 Implementation	35
7.1 Existing Routines	35
7.2 Implementation of the new Detection Routines	36
7.3 Implementation of the Regularization Strategy	36
8 Results	39
8.1 Diffusion Test	39
8.2 Flume Experiment	41
8.3 Field Application	46
9 Recommendations	53
10 Conclusions	55
A Sediment Transport Closure Relations and its Derivatives	57
A.1 Nondimensional Sediment Transport	57
A.1.1 <i>Ashida and Michiue</i> (1971) Nondimensional Sediment Transport	57
A.1.2 <i>Engelund and Hansen</i> (1967) Nondimensional Sediment Transport	57
A.2 Hiding Relations	57
A.2.1 <i>Ashida and Michiue</i> (1971) Hiding Relation	58

Deltares

A.3	Mean Grain Size	58
A.3.1	Arithmetic Mean Grain Size	58
A.3.2	Geometric Mean Grain Size	58
B	Proof that a Modification of the Time Scale of Mixing does not Regularize the 2D Model	61
C	Proof that Diffusion in Hirano Regularizes the 2D Model	63

List of Tables

5.1	Reference state.	24
5.2	Cases of a stable well-posed model (I1), an unstable well-posed model (B1), and an ill-posed model (I2). Case I2 has the same parameter values as Case I1 but for the mean flow velocity which is equal to 6.30 m/s.	24
5.3	Cases showing the effect of grid cell size on the numerical solution of well-posed and ill-posed models.	27

1 Introduction

Modelling of fluvial morphodynamic processes is a powerful tool not only to predict the future state of a river after, for instance, an intervention or a change in the discharge regime (*Blom et al.*, 2017), but also as a source of understanding of the natural processes responsible for patterns such as dunes, meanders, and bars (*Callander*, 1969; *Seminara*, 2006; *Colombini and Stocchino*, 2012). A framework for modelling the morphodynamic development of alluvial rivers is composed of a system of partial differential equations for modelling the flow, change in bed elevation, and change in the bed surface texture. The *Saint-Venant* (1871) equations account for conservation of water mass and momentum and enable modelling processes with a characteristic length scale significantly longer than the flow depth in one-dimensional cases. The Shallow Water Equations describe the depth-averaged flow in two-dimensional cases. Conservation of unisize bed sediment is typically modelled using the *Exner* (1920) equation and, under mixed-size sediment conditions, the active layer model (*Hirano*, 1971) accounts for mass conservation of bed sediment of each grain size.

Although widely successful in predicting river morphodynamics, a fundamental problem arises when using the above framework. Under certain conditions the description of the natural phenomena is not captured by the system of equations, which manifests as an ill-posed model. Models describe a simplified version of reality, which allows us to understand the key elements playing a major role in the dynamics of the system one studies (*Paola and Leeder*, 2011). Major simplifications such as reducing streamwise morphodynamic processes to a diffusion equation allow for insight on the creation of stratigraphic records and evolution on large spatial scales (*Paola et al.*, 1992; *Paola*, 2000; *Paola and Leeder*, 2011). There is a difference between greatly simplified models and models that do not capture the physical processes. A simplified model reproduces a reduced-complexity version of reality (*Murray*, 2007) and it is mathematically well-posed, as a unique solution exists that depends continuously on the data (*Hadamard*, 1923; *Joseph and Saut*, 1990). An ill-posed model lacks crucial physical processes that cause the model to be unsuitable to capture the dynamics of the system (*Fowler*, 1997). An ill-posed model is unrepresentative of a physical phenomenon, as the growth rate of infinitesimal perturbations to a solution (i.e., negligible noise from a physical perspective) tends to infinity (*Kabanikhin*, 2008). This is different from chaotic systems, in which noise similarly causes the solution to diverge but not infinitely fast (*Devaney*, 1989; *Banks et al.*, 1992).

An example of an ill-posed model is the one describing the dynamics of granular flow. The continuum formulation of such a problem depends on deriving a model for the granular viscosity. *Jop et al.* (2005, 2006) relate viscosity to a dimensionless shear rate. The model captures the dynamics of granular flows if the dimensionless shear rate is within a certain range, but otherwise the model is ill-posed and loses its predictive capabilities (*Barker et al.*, 2015). A better representation of the physical processes guaranteeing that viscosity tends to 0 when the dimensionless shear rate tends to 0 extends the domain of well-posedness (*Barker and Gray*, 2017).

Under unisize sediment and one-dimensional flow conditions, the Saint-Venant-Exner model may be ill-posed when the Froude number is larger than 6 (*Cordier et al.*, 2011). As most flows of interest are well below this limit, we can consider modelling of fluvial problems under unisize sediment conditions to be well-posed. This is not the case when considering mixed-size sediment. Using the active layer model we assume that the bed can be discretised into two layers: the active layer and the substrate. The sediment transport rate depends on the grain size distribution of the active layer. A vertical flux of sediment occurs between the active layer and the substrate if the elevation of the interface between the active layer and the

substrate changes. The active layer is well-mixed, whereas the substrate can be stratified. The above simplification of the physical processes responsible for vertical mixing causes the active layer model to be ill-posed (*Ribberink, 1987; Stecca et al., 2014; Chavarrías et al., 2018*). In particular, the active layer is prone to be ill-posed under degradational conditions into a substrate finer than the active layer (i.e., an armoured bed (*Parker and Sutherland, 1990*)) for any value of the Froude number.

Chavarrías et al. (2019b) devised a regularization strategy to guarantee that the active layer model is unconditionally well-posed. The strategy can be classified as a preconditioning technique (*Turkel, 1999*) and is based on modifying the time scale of mixing processes. *Chavarrías et al. (2019b)* proved that, under conditions in which the active layer model is ill-posed, the system is regularized by sufficiently slowing down the mixing processes. The physical interpretation of the strategy is that the active layer model is ill-posed when it becomes incapable of capturing fast mixing processes occurring in nature under the conditions in which the model is ill-posed. The slow down of the mixing processes implies an increase in the time scale under consideration. Worded differently, the time scale over which the model variables are representative of the conditions of the bed is increased.

Chavarrías et al. (2019b) tested the results of the regularization strategy against data from laboratory experiments and confirmed that the regularized active layer model captures the behavior of the system averaged over the passage of several bedforms causing fast mixing of sediment. Yet, the strategy was devised under one-dimensional conditions only. In this document we propose a regularization strategy that guarantees that the two-dimensional active layer model is well-posed.

The document is organized as follows. In Section 2 we introduce the active layer model. In Section 3 we propose two regularization strategies. In Section 4 we linearize the model to be able to conduct a perturbation analysis in Section 5. Analytical results of the perturbation analysis are described in Section 6. In Section 7 we discuss the implementation of the regularization strategy in Delft3D. The results of applying the regularization strategy are shown in Section 8. Recommendations and conclusions are found in Sections 9 and 10, respectively.

2 Original Model Equations

In this section we describe the set of equations used in modelling mixed-size sediment morphodynamic processes. In Section 2.1 we introduce the conservation equations and in Section 2.2 the closure relations of the model.

2.1 Conservation Equations

In this section we describe the conservation equations of the model. In Sections 2.1.1 and 2.1.2 we introduce the equations accounting for changes in the flow and in the bed, respectively.

2.1.1 Flow Equations

We assume that the vertical length and velocity scales are negligible with respect to the horizontal ones. Another assumption is the fact that the concentration of sediment (the ratio between the solid and liquid discharge) is small (below 6×10^{-3} (Garegnani *et al.*, 2011, 2013)), such that we apply the clear water approximation. Under these conditions, the flow is described using the depth-averaged Shallow Water Equations (e.g. Vreugdenhil, 1994):

$$\frac{\partial h}{\partial t} + \frac{\partial q_x}{\partial x} + \frac{\partial q_y}{\partial y} = 0, \quad (2.1)$$

$$\begin{aligned} & \frac{\partial q_x}{\partial t} + \frac{\partial(q_x^2/h + gh^2/2)}{\partial x} + \frac{\partial(\frac{q_x q_y}{h})}{\partial y} + gh \frac{\partial \eta}{\partial x} - F_{sx} = \\ & = 2 \frac{\partial}{\partial x} \left(\nu h \frac{\partial(\frac{q_x}{h})}{\partial x} \right) + \frac{\partial}{\partial y} \left(\nu h \left(\frac{\partial(\frac{q_x}{h})}{\partial y} + \frac{\partial(\frac{q_y}{h})}{\partial x} \right) \right) - gh S_{fx}, \end{aligned} \quad (2.2)$$

$$\begin{aligned} & \frac{\partial q_y}{\partial t} + \frac{\partial(q_y^2/h + gh^2/2)}{\partial y} + \frac{\partial(\frac{q_x q_y}{h})}{\partial x} + gh \frac{\partial \eta}{\partial y} - F_{sy} = \\ & 2 \frac{\partial}{\partial y} \left(\nu h \frac{\partial(\frac{q_y}{h})}{\partial y} \right) + \frac{\partial}{\partial x} \left(\nu h \left(\frac{\partial(\frac{q_y}{h})}{\partial x} + \frac{\partial(\frac{q_x}{h})}{\partial y} \right) \right) - gh S_{fy}, \end{aligned} \quad (2.3)$$

where (x, y) [m] are Cartesian coordinates and t [s] is the time coordinate. The variables $(q_x, q_y) = (uh, vh)$ [m²/s] are the specific water discharges in the x and y direction, respectively, where h [m] is the flow depth and u [m/s] and v [m/s] are the depth-averaged flow velocities. The variable η [m] is the bed elevation and g [m/s²] the acceleration due to gravity. The friction slopes are (S_{fx}, S_{fy}) [–] and the diffusion coefficient ν [m²/s] is the horizontal eddy viscosity. The depth-averaging procedure of the equations of motion introduces terms that originate from the difference between the actual velocity at a certain elevation in the water column and the depth-averaged velocity. We separate the contributions due to turbulent motion and secondary flow caused by the flow curvature. The contribution due to turbulent motion is accounted for by the diffusion coefficient. The terms (F_{sx}, F_{sy}) [m²/s²] account for the effect of secondary flow. These terms are responsible for a transfer of momentum that shifts the maximum velocity to the outer bend (Kalkwijk and De Vriend, 1980), as well as for a sink of energy in the secondary circulation (Flokstra, 1977; Begnudelli *et al.*, 2010).

The integral value (along z) of the force per unit mass that the secondary flow exerts on the primary flow is (De Vriend, 1977; Kalkwijk and De Vriend, 1980):

$$F_{sx} = \frac{\partial T_{xx}}{\partial x} + \frac{\partial T_{xy}}{\partial y}, \quad (2.4)$$

$$F_{sy} = \frac{\partial T_{yx}}{\partial x} + \frac{\partial T_{yy}}{\partial y}, \quad (2.5)$$

where T_{lm} [m^3/s^2] is the integral shear stress per unit mass in the direction l - m . Assuming a large width-to-depth ratio (i.e., $B/h \gg 1$, where B [m] is the characteristic channel width) and a mild curvature (i.e., $h/R_s \ll 1$, where R_s [m] is the radius of curvature of the streamlines), the shear stress terms are:

$$T_{xx} = -2 \frac{\beta^* I}{Q} q_x q_y, \quad (2.6)$$

$$T_{xy} = T_{yx} = \frac{\beta^* I}{Q} (q_x^2 - q_y^2), \quad (2.7)$$

$$T_{yy} = T_{yy} = 2 \frac{\beta^* I}{Q} q_x q_y, \quad (2.8)$$

where $\beta^* = 5\alpha - 15.6\alpha^2 + 37.5\alpha^3$ and I [m/s] is the secondary flow intensity, which is the integral of the absolute value of the secondary flow velocity profile (*De Vriend, 1981*), and $Q = \sqrt{q_x^2 + q_y^2}$ [m^2/s] is the module of the specific water discharge.

The secondary flow intensity varies in space and time and it is modelled by means of an advection-diffusion equation (*Jagers, 2003*). *Chavarrías et al. (2019a)* showed that the diffusion coefficient of the transport equation of the secondary flow intensity is a crucial parameter to guarantee well-posedness of the flow equations. They also showed that ill-posedness as regards to modelling of the sediment mixing processes is independent from secondary flow modelling and from the diffusion in the flow equations. Worded differently, ill-posedness due to the active layer model is independent of ill-posedness due to secondary flow. For this reason, as we are here concerned about regularizing the active layer model, we will not consider the secondary flow intensity as a dependent variable of the model. This implies that we assume that the effect of spatial and temporal changes in secondary flow intensity are negligible. Similarly, we will neglect the effect of diffusion in the flow equations, as it has been shown to not play a role in the well-posedness of the active layer model (*Chavarrías et al., 2019a*).

2.1.2 Morphodynamic Equations

We consider an alluvial bed composed of an arbitrary number N of non-cohesive sediment fractions characterised by a grain size d_k [m], where the subscript k denotes the grain size fraction in increasing order (i.e., $d_1 < d_2 < \dots < d_N$). Bed elevation change depends on the divergence of the sediment transport rate (*Exner, 1920*):

$$\frac{\partial \eta}{\partial t} + \frac{\partial q_{bx}}{\partial x} + \frac{\partial q_{by}}{\partial y} = 0, \quad (2.9)$$

where $q_{bx} = \sum_{k=1}^N q_{bxk}$ [m^2/s] and $q_{by} = \sum_{k=1}^N q_{byk}$ [m^2/s] are the total specific (i.e., per unit of differential length) sediment transport rates including pores in the x and y direction, respectively. The variables q_{bxk} [m^2/s] and q_{byk} [m^2/s] are the specific sediment transport rates of size fraction k including pores. For simplicity we assume a constant porosity and density of the bed sediment. The sediment transport rate is assumed to be locally at capacity, which implies that we do not model the temporal and spatial adaptation of the sediment transport

rate to capacity conditions (*Bell and Sutherland, 1983; Phillips and Sutherland, 1989; Jain, 1992*).

Changes in the bed surface grain size distribution are accounted for using the active layer model (*Hirano, 1971*). Conservation of sediment mass of size fraction k in the active layer reads:

$$\frac{\partial M_{ak}}{\partial t} + f_k^I \frac{\partial (\eta - L_a)}{\partial t} + \frac{\partial q_{bxk}}{\partial x} + \frac{\partial q_{byk}}{\partial y} = 0 \quad k \in \{1, N - 1\}, \quad (2.10)$$

and in the substrate (*Chavarrías et al., 2018*):

$$\frac{\partial M_{sk}}{\partial t} - f_k^I \frac{\partial (\eta - L_a)}{\partial t} = 0 \quad k \in \{1, N - 1\}, \quad (2.11)$$

where $M_{ak} = F_{ak} L_a$ [m] and $M_{sk} = \int_{\eta_0}^{\eta_0 + \eta - L_a} f_{sk}(z) dz$ [m] are the volume of sediment of size fraction k per unit of bed area in the active layer and the substrate, respectively. Parameter η_0 [m] is a datum for bed elevation. Parameters $F_{ak} \in [0, 1]$, $f_{sk} \in [0, 1]$, and $f_k^I \in [0, 1]$ are the volume fraction content of sediment of size fraction k in the active layer, substrate, and at the interface between the active layer and the substrate, respectively. By definition, the sum of the volume fraction content over all size fractions equals 1:

$$\sum_{k=1}^N F_{ak} = 1, \quad \sum_{k=1}^N f_{sk}(z) = 1, \quad \sum_{k=1}^N f_k^I = 1. \quad (2.12)$$

The active layer thickness represents the part of the bed assumed to be instantaneously and perfectly mixed. The active layer thickness has not vertical stratification. For this reason, the active layer thickness depends on the time scale under consideration (*Bennett and Nordin, 1977; Rahuel et al., 1989; Sieben, 1997; Wu, 2007*). Under plain bed conditions, the active layer thickness is usually related to the grain size distribution of the bed surface (*Petts et al., 1989; Rahuel et al., 1989*). Under bedform dominated conditions, the part of the bed that plays an active role in the sediment transport processes is usually related to a characteristic bedform height (*Deigaard and Fredsøe, 1978; Lee and Odgaard, 1986; Armanini and Di Silvio, 1988*). A more accurate representation of the mixing processes may be obtained if the active layer thickness varies in space and time according to the local properties of the bed and the flow. This approach implies that the active layer thickness is a dependent variable of the system. *Chavarrías et al. (2018)* showed that when considering a variable active layer thickness depending on the flow depth to account for the dependence on dune height, the domain in which the active layer model is ill-posed increases slightly. Yet, the main cause of ill-posedness is independent of considering a variable active layer thickness (*Chavarrías et al., 2018*). For this reason, here we assume a constant active layer thickness.

2.2 Closure Relations

The model introduced in Section 2.1 requires closure relations for the friction slope, the volume fraction content of sediment at the interface between the active layer and the substrate, and the sediment transport rate. In this section we describe the closure relations of the model.

We assume a Chézy-type friction such that:

$$S_{fx} = \frac{C_f q_x Q}{gh^3}, \quad S_{fy} = \frac{C_f q_y Q}{gh^3}, \quad (2.13)$$

where parameter C_f [–] is a nondimensional friction coefficient, which we assume to be constant (*Ikeda et al., 1981; Schielen et al., 1993*). In general, the friction coefficient depends

on the flow depth and grain size. The consequences of this decision are discussed in Section 9.

Under degradational conditions, the volume fraction content of size fraction k at the interface between the active layer and the substrate is equal to that at the top part of the substrate ($f_k^1 = f_{sk}(z = \eta - L_a)$ for $\partial\eta/\partial t < 0$). This allows for modelling of arbitrarily abrupt changes in grain size due to erosion of previous deposits. Under aggradational conditions the sediment transferred to the substrate is a weighted mixture of the sediment in the active layer and the bed load (Parker, 1991; Hoey and Ferguson, 1994; Toro-Escobar et al., 1996). Here we simplify the analysis and we assume that the contribution of the bed load to the depositional flux is negligible (i.e., $f_k^1 = F_{ak}$ for $\partial\eta/\partial t > 0$) (Hirano, 1971).

The module of the specific sediment transport rate of size fraction k , q_{bk} [m²/s], has a direction given by the angle φ_{sk} [rad]:

$$(q_{bxk}, q_{byk}) = q_{bk}(\cos \varphi_{sk}, \sin \varphi_{sk}) . \quad (2.14)$$

The magnitude of the sediment transport rate is equal to:

$$q_{bk} = F_{ak} \frac{\sqrt{gRd_k^3}}{(1-p)} q_{bk}^* , \quad (2.15)$$

where p is the porosity and q_{bk}^* [–] is a nondimensional sediment transport rate (Einstein, 1950). The nondimensional sediment transport rate is computed using relations such as the ones derived by Meyer-Peter and Müller (1948); Engelund and Hansen (1967); Ashida and Michiue (1971), or Wilcock and Crowe (2003). These relations depend on the nondimensional bed shear stress (or Shields (1936) stress):

$$\theta_k = \frac{C_f \left(\frac{Q}{h}\right)^2}{gRd_k} , \quad (2.16)$$

where parameter $R = \rho_s/\rho_w - 1$ [–] is the submerged sediment density, $\rho_s = 2650 \text{ kg/m}^3$ is the sediment density and $\rho_w = 1000 \text{ kg/m}^3$ is the water density. The relations for the nondimensional sediment transport rate may depend on a hiding factor ξ_k [–], that accounts for the fact that fine sediment in a mixture hides behind larger grains and a coarse sediment in a mixture is more exposed than in unisize coarse sediment (Einstein, 1950). The hiding factor depends on the mean grain size of the bed surface D_m [–]. In Appendix A we present several closure relations for nondimensional sediment transport rate, hiding, and the mean grain size.

The direction of the sediment transport (φ_{sk} [rad]) is affected by the secondary flow and the bed slope (Van Bendegom, 1947):

$$\tan \varphi_{sk} = \frac{\sin \varphi_\tau - \frac{1}{g_{sk}} \frac{\partial \eta}{\partial y}}{\cos \varphi_\tau - \frac{1}{g_{sk}} \frac{\partial \eta}{\partial x}} \quad k \in \{1, N\} , \quad (2.17)$$

where g_{sk} [–] is a function that accounts for the influence of the bed slope on the sediment transport direction and φ_τ [rad] is the direction of the sediment transport accounting for the secondary flow only:

$$\tan \varphi_\tau = \frac{q_y - h\alpha_I \frac{q_x}{Q} I}{q_x - h\alpha_I \frac{q_y}{Q} I} . \quad (2.18)$$

Assuming a mild curvature, uniform flow conditions, and a logarithmic profile of the primary flow, the constant $\alpha_I [-]$ is (*De Vriend, 1977*):

$$\alpha_I = \frac{2}{\kappa^2} (1 - \alpha) . \quad (2.19)$$

The effect of the bed slope on the sediment transport direction depends on the grain size (*Parker and Andrews, 1985*). We account for this effect setting:

$$g_{sk} = A_s \theta_k^{B_s} \quad k \in \{1, N\} , \quad (2.20)$$

where $A_s [-]$ and $B_s [-]$ are nondimensional parameters. Different values of the coefficients A_s and B_s have been proposed (for a recent review, see *Baar et al. (2018)*).

3 Regularization Strategy

In this section we discuss two regularization strategies. In Section 3.1 we describe the extension to two-dimensional conditions of the regularization strategy devised by *Chavarrías et al. (2019b)*. In Section 3.2 we introduce a new regularization strategy.

3.1 Modification of the Time Scale of Mixing Processes

In this section we describe the possible regularization strategy based on a modification of the time scale of the mixing processes. This strategy is a direct extension to two dimensions of the strategy by *Chavarrías et al. (2019b)*. The strategy modifies the active layer equation only and is equivalent to using a preconditioning technique. One important limitation of this strategy is that it can only be used when the active layer thickness is constant. The modification consist of introducing a factor $\alpha [-]$ multiplying the rate of temporal change of the volume of sediment in the active layer:

$$\alpha \frac{\partial M_{ak}}{\partial t} + f_k^I \frac{\partial (\eta - L_a)}{\partial t} + \frac{\partial q_{bxk}}{\partial x} + \frac{\partial q_{byk}}{\partial y} = 0 \quad k \in \{1, N-1\}. \quad (3.1)$$

3.2 Addition of Diffusion to the Active Layer Equation

In this section we propose an alternative regularization strategy to the extension to two dimension of the strategy by *Chavarrías et al. (2019b)*. The modification of the time scales that successfully regularizes the one-dimensional model has the physical implication of filtering the small time scale processes. We pursue a strategy that similarly implicitly accounts for the small time scale processes.

We consider that the small time scale processes of sediment mixing in the active layer are represented by an additional diffusive flux. This is similar to accounting for the small time scale processes of water movement (i.e., turbulence), by means considering additional viscosity (i.e., eddy viscosity). The proposed modified active layer equation is:

$$\frac{\partial M_{ak}}{\partial t} + f_k^I \frac{\partial (\eta - L_a)}{\partial t} + \frac{\partial q_{bxk}}{\partial x} + \frac{\partial q_{byk}}{\partial y} - \kappa_{Hx} \frac{\partial^2 M_{ak}}{\partial x^2} - \kappa_{Hy} \frac{\partial^2 M_{ak}}{\partial y^2} = 0 \quad k \in \{1, N-1\}, \quad (3.2)$$

where $\kappa_{Hx} > 0$ [m²/s] and $\kappa_{Hy} > 0$ [m²/s] are diffusion coefficients in the x and y direction, respectively.

While we compare the additional diffusive flux with turbulent diffusion, we are not explicitly deriving the flux from filtering small scale perturbations, as one can do for deriving the turbulent diffusive flux. This exercise would strengthen the theoretical basis of the proposed equation.

We see no reason to limit the active layer thickness to be constant with time. This is because mass is conserved regardless of the time variation of the active layer thickness.

4 Linearization of the System of Equations

In assessing the well-posedness of the system of equations, we will consider growth of perturbations in the linear model. In this section we present the linearized system of equations. We subsequently summarize the model equations.

The system models the evolution of $N+3$ variables: h, q_x, q_y, η , and $M_{ak} \forall k \in \{1, N-1\}$. The model equations are:

$$\frac{\partial h}{\partial t} + \frac{\partial q_x}{\partial x} + \frac{\partial q_y}{\partial y} = 0, \quad (4.1)$$

$$\frac{\partial q_x}{\partial t} + \frac{\partial(q_x^2/h + gh^2/2)}{\partial x} + \frac{\partial\left(\frac{q_x q_y}{h}\right)}{\partial y} + gh \frac{\partial \eta}{\partial x} - F_{sx} = -ghS_{fx}, \quad (4.2)$$

$$\frac{\partial q_y}{\partial t} + \frac{\partial(q_y^2/h + gh^2/2)}{\partial y} + \frac{\partial\left(\frac{q_x q_y}{h}\right)}{\partial x} + gh \frac{\partial \eta}{\partial y} - F_{sy} = -ghS_{fy}, \quad (4.3)$$

$$\frac{\partial \eta}{\partial t} + \frac{\partial q_{bx}}{\partial x} + \frac{\partial q_{by}}{\partial y} = 0, \quad (4.4)$$

For the case of the first regularization strategy, the active layer equation is:

$$\alpha \frac{\partial M_{ak}}{\partial t} - f_k^I \frac{\partial q_{bx}}{\partial x} - f_k^I \frac{\partial q_{by}}{\partial y} + \frac{\partial q_{bxk}}{\partial x} + \frac{\partial q_{byk}}{\partial y} = 0 \quad k \in \{1, N-1\}. \quad (4.5)$$

For the case of the second regularization strategy, the active layer equation is:

$$\frac{\partial M_{ak}}{\partial t} - f_k^I \frac{\partial q_{bx}}{\partial x} - f_k^I \frac{\partial q_{by}}{\partial y} + \frac{\partial q_{bxk}}{\partial x} + \frac{\partial q_{byk}}{\partial y} - \kappa_{Hx} \frac{\partial^2 M_{ak}}{\partial x^2} - \kappa_{Hy} \frac{\partial^2 M_{ak}}{\partial y^2} = 0 \quad k \in \{1, N-1\}. \quad (4.6)$$

We consider a reference state that is a solution to the system of equations. The reference state is a steady uniform straight flow in the x direction over an inclined plane bed composed of an arbitrary number of size fractions. Mathematically: $h_0 = \text{ct.}$, $q_{x0} = \text{ct.}$, $q_{y0} = 0$, $\frac{\partial \eta}{\partial x} = \text{ct.} = \frac{-C_I q_{x0}^2}{gh_0^3}$, $\frac{\partial \eta}{\partial y} = 0$, $M_{ak0} = \text{ct.} \forall k \in \{1, N-1\}$, where ct. denotes a constant different from 0 and subscript 0 indicates the reference solution. A small perturbation $h', q'_x, q'_y, \eta', M'_{ak} \forall k \in \{1, N-1\}$ is added to the reference solution.

The linearization of Equations (4.1)-(4.6) is conducted in Sections 4.1-4.5.

4.1 Water Mass Conservation

The non-linear equation is:

$$\frac{\partial h}{\partial t} + \frac{\partial q_x}{\partial x} + \frac{\partial q_y}{\partial y} = 0 \quad (4.7)$$

Linearizing and substituting the reference solution we obtain:

$$\frac{\partial h'}{\partial t} + \frac{\partial q'_x}{\partial x} + \frac{\partial q'_y}{\partial y} = 0 \quad (4.8)$$

4.2 Water Momentum Conservation in x Direction

The non-linear equation is:

$$\begin{aligned} \frac{\partial q_x}{\partial t} + \frac{\partial(q_x^2/h + gh^2/2)}{\partial x} + gh \frac{\partial \eta}{\partial x} - F_{sx} \\ + \frac{\partial \left(\frac{q_x q_y}{h} \right)}{\partial y} \\ + gh S_{fx} = 0 . \end{aligned} \quad (4.9)$$

Expanding the terms we obtain:

$$\begin{aligned} \frac{\partial q_x}{\partial t} + \left(gh - \left(\frac{q_x}{h} \right)^2 \right) \frac{\partial h}{\partial x} + \left(2 \frac{q_x}{h} - \frac{\partial T_{xx}}{\partial q_x} \right) \frac{\partial q_x}{\partial x} - \frac{\partial T_{xx}}{\partial q_y} \frac{\partial q_y}{\partial x} + gh \frac{\partial \eta}{\partial x} \\ - \frac{q_x q_y}{h^2} \frac{\partial h}{\partial y} + \left(\frac{q_y}{h} - \frac{\partial T_{xy}}{\partial q_x} \right) \frac{\partial q_x}{\partial y} + \left(\frac{q_x}{h} - \frac{\partial T_{xy}}{\partial q_y} \right) \frac{\partial q_y}{\partial y} \\ + \frac{C_f q_x Q}{h^2} = 0 . \end{aligned} \quad (4.10)$$

Linearizing and substituting the reference solution we obtain:

$$\begin{aligned} \frac{\partial q'_x}{\partial t} + \left(gh_0 - \left(\frac{q_{x0}}{h_0} \right)^2 \right) \frac{\partial h'}{\partial x} + 2 \frac{q_{x0}}{h_0} \frac{\partial q'_x}{\partial x} + gh_0 \frac{\partial \eta'}{\partial x} + gh' \frac{\partial \eta_0}{\partial x} \\ + \frac{q_{x0}}{h_0} \frac{\partial q'_y}{\partial y} \\ - \frac{2C_f q_{x0}^2}{h_0^3} h' + \frac{2C_f q_{x0}}{h_0^2} q'_x = 0 . \end{aligned} \quad (4.11)$$

Reorganizing the terms we obtain:

$$\begin{aligned} \frac{\partial q'_x}{\partial t} + \left(gh_0 - \left(\frac{q_{x0}}{h_0} \right)^2 \right) \frac{\partial h'}{\partial x} + 2 \frac{q_{x0}}{h_0} \frac{\partial q'_x}{\partial x} + gh_0 \frac{\partial \eta'}{\partial x} \\ + \frac{q_{x0}}{h_0} \frac{\partial q'_y}{\partial y} \\ + \left(g \frac{\partial \eta_0}{\partial x} - \frac{2q_{x0}^2}{h_0^3} \right) h' + \frac{2q_{x0}}{h_0^2} q'_x = 0 . \end{aligned} \quad (4.12)$$

In all the terms multiplying a derivative with reference solution equal to zero, only the zero order part is not negligible. For instance, expanding in Taylor series until the first order, the first term of the momentum equation in the x direction is:

$$gh - \left(\frac{q_x}{h} \right)^2 = gh_0 - \left(\frac{q_{x0}}{h_0} \right)^2 + \left(g + \frac{2q_{x0}^2}{h_0^3} \right) h' - \frac{2q_{x0}}{h_0} q'_x . \quad (4.13)$$

Multiplying by the derivative we obtain:

$$\left(gh_0 - \left(\frac{q_{x0}}{h_0} \right)^2 + \left(g + \frac{2q_{x0}^2}{h_0^3} \right) h' - \frac{2q_{x0}}{h_0} q'_x \right) \frac{\partial h'}{\partial x} = \left(gh_0 - \left(\frac{q_{x0}}{h_0} \right)^2 \right) \frac{\partial h'}{\partial x} , \quad (4.14)$$

where we have neglected second order terms. The terms multiplying the bed slope (the derivative of the reference solution is not equal to zero) are:

$$gh \frac{\partial \eta}{\partial x} = g(h_0 + h') \frac{\partial(\eta_0 + \eta')}{\partial x} = gh_0 \frac{\partial \eta_0}{\partial x} + gh_0 \frac{\partial \eta'}{\partial x} + gh' \frac{\partial \eta_0}{\partial x}, \quad (4.15)$$

where we have neglected secondary terms. The linearization of the friction term is:

$$\frac{C_f q_x Q}{h^2} = \frac{C_f q_{x0}^2}{h_0^2} - \frac{2C_f q_{x0}^2}{h_0^3} h' + \frac{2C_f q_{x0}}{h_0^2} q'_x. \quad (4.16)$$

We have used that:

$$\left. \frac{\partial T_{xx}}{\partial q_x} \right|_0 = 0 \quad (4.17)$$

$$\left. \frac{\partial T_{xx}}{\partial q_y} \right|_0 = 0 \quad (4.18)$$

$$\left. \frac{\partial T_{xy}}{\partial q_x} \right|_0 = 0 \quad (4.19)$$

$$\left. \frac{\partial T_{xy}}{\partial q_y} \right|_0 = 0 \quad (4.20)$$

4.3 Water Momentum Conservation in y Direction

The non-linear equation is:

$$\begin{aligned} & \frac{\partial q_y}{\partial t} + \frac{\partial \left(\frac{q_x q_y}{h} \right)}{\partial x} \\ & + \frac{\partial (q_y^2/h + gh^2/2)}{\partial y} + gh \frac{\partial \eta}{\partial y} - F_{sy} \\ & + gh S_{fy} = 0. \end{aligned} \quad (4.21)$$

Expanding the terms we obtain:

$$\begin{aligned} & \frac{\partial q_y}{\partial t} - \frac{q_x q_y}{h^2} \frac{\partial h}{\partial x} + \left(\frac{q_y}{h} - \frac{\partial T_{yx}}{\partial q_x} \right) \frac{\partial q_x}{\partial x} + \left(\frac{q_x}{h} - \frac{\partial T_{yx}}{\partial q_y} \right) \frac{\partial q_y}{\partial x} \\ & + \left(gh - \left(\frac{q_y}{h} \right)^2 \right) \frac{\partial h}{\partial y} - \frac{\partial T_{yy}}{\partial q_x} \frac{\partial q_x}{\partial y} + \left(2 \frac{q_y}{h} - \frac{\partial T_{yy}}{\partial q_y} \right) \frac{\partial q_y}{\partial y} + gh \frac{\partial \eta}{\partial y} \\ & + \frac{C_f q_y Q}{h^2} = 0 \end{aligned} \quad (4.22)$$

Linearizing and substituting the reference solution we obtain:

$$\begin{aligned} & \frac{\partial q'_y}{\partial t} + \frac{q_{x0}}{h_0} \frac{\partial q'_y}{\partial x} \\ & + gh_0 \frac{\partial h'}{\partial y} + gh_0 \frac{\partial \eta'}{\partial y} \\ & \frac{C_f q_{x0}}{h_0^2} q'_y = 0. \end{aligned} \quad (4.23)$$

4.4 Sediment Mass Conservation for the Entire Mixture

The non-linear equation is:

$$\frac{\partial \eta}{\partial t} + \frac{\partial q_{bx}}{\partial x} + \frac{\partial q_{by}}{\partial y} = 0 \quad (4.24)$$

Expanding the terms we obtain:

$$\begin{aligned} \frac{\partial \eta}{\partial t} + \frac{\partial q_{bx}}{\partial h} \frac{\partial h}{\partial x} + \frac{\partial q_{bx}}{\partial q_x} \frac{\partial q_x}{\partial x} + \frac{\partial q_{bx}}{\partial q_y} \frac{\partial q_y}{\partial x} + \sum_{l=1}^{N-1} \frac{\partial q_{bx}}{\partial M_{al}} \frac{\partial M_{al}}{\partial x} \\ + \frac{\partial q_{by}}{\partial h} \frac{\partial h}{\partial y} + \frac{\partial q_{by}}{\partial q_x} \frac{\partial q_x}{\partial y} + \frac{\partial q_{by}}{\partial q_y} \frac{\partial q_y}{\partial y} + \sum_{l=1}^{N-1} \frac{\partial q_{by}}{\partial M_{al}} \frac{\partial M_{al}}{\partial y} \\ + \frac{\partial q_{bx}}{\partial \frac{\partial \eta}{\partial x}} \frac{\partial^2 \eta}{\partial x^2} + \frac{\partial q_{bx}}{\partial \frac{\partial \eta}{\partial y}} \frac{\partial^2 \eta}{\partial x \partial y} + \frac{\partial q_{by}}{\partial \frac{\partial \eta}{\partial x}} \frac{\partial^2 \eta}{\partial x \partial y} + \frac{\partial q_{by}}{\partial \frac{\partial \eta}{\partial y}} \frac{\partial^2 \eta}{\partial y^2}, \end{aligned} \quad (4.25)$$

where we have used that:

$$q_{bxk} = f \left(h, q_x, q_y, M_{ak}, \frac{\partial \eta}{\partial x}, \frac{\partial \eta}{\partial y} \right). \quad (4.26)$$

Note that q_{bxk} is not a function of the bed elevation η , but it is a function of the derivatives of η . For a function $f \left(\eta, \frac{\partial \eta}{\partial x} \right)$ we write:

$$\frac{\partial f}{\partial x} = \frac{\partial f}{\partial \eta} \frac{\partial \eta}{\partial x} + \frac{\partial f}{\partial \frac{\partial \eta}{\partial x}} \frac{\partial^2 \eta}{\partial x^2}. \quad (4.27)$$

In the linearization, all the derivatives are evaluated at the reference state only and no other terms appear. This is because the only variable whose derivative is not equal to 0 in the reference state is η , but the sediment transport rate does not depend on η . For instance:

$$\begin{aligned} \frac{\partial q_{bxk}}{\partial h} \frac{\partial h}{\partial x} = \frac{\partial q_{bxk}}{\partial h} \Big|_{\mathbf{Q}_0 + \mathbf{Q}'} \frac{\partial (h_0 + h')}{\partial x} = \\ \left[\frac{\partial q_{bxk}}{\partial h} \Big|_{\mathbf{Q}_0} + h' \frac{\partial^2 q_{bxk}}{\partial h^2} \Big|_{\mathbf{Q}_0} + q'_x \frac{\partial^2 q_{bxk}}{\partial h \partial q_x} \Big|_{\mathbf{Q}_0} + \dots \right] \left(\frac{\partial h_0}{\partial x} + \frac{\partial h'}{\partial x} \right) = \\ \frac{\partial q_{bxk}}{\partial h} \Big|_{\mathbf{Q}_0} \frac{\partial h'}{\partial x} \end{aligned} \quad (4.28)$$

We will denote $|_{\mathbf{Q}_0} = |_0$. Therefore, the linearized equation is:

$$\begin{aligned} \frac{\partial \eta'}{\partial t} + \frac{\partial q_{bx}}{\partial h} \Big|_0 \frac{\partial h}{\partial x} + \frac{\partial q_{bx}}{\partial q_x} \Big|_0 \frac{\partial q_x}{\partial x} + \frac{\partial q_{bx}}{\partial q_y} \Big|_0 \frac{\partial q_y}{\partial x} + \sum_{l=1}^{N-1} \frac{\partial q_{bx}}{\partial M_{al}} \Big|_0 \frac{\partial M_{al}}{\partial x} \\ + \frac{\partial q_{by}}{\partial h} \Big|_0 \frac{\partial h}{\partial y} + \frac{\partial q_{by}}{\partial q_x} \Big|_0 \frac{\partial q_x}{\partial y} + \frac{\partial q_{by}}{\partial q_y} \Big|_0 \frac{\partial q_y}{\partial y} + \sum_{l=1}^{N-1} \frac{\partial q_{by}}{\partial M_{al}} \Big|_0 \frac{\partial M_{al}}{\partial y} \\ + \frac{\partial q_{bx}}{\partial \frac{\partial \eta}{\partial x}} \Big|_0 \frac{\partial^2 \eta}{\partial x^2} + \frac{\partial q_{bx}}{\partial \frac{\partial \eta}{\partial y}} \Big|_0 \frac{\partial^2 \eta}{\partial x \partial y} + \frac{\partial q_{by}}{\partial \frac{\partial \eta}{\partial x}} \Big|_0 \frac{\partial^2 \eta}{\partial x \partial y} + \frac{\partial q_{by}}{\partial \frac{\partial \eta}{\partial y}} \Big|_0 \frac{\partial^2 \eta}{\partial y^2}, \end{aligned} \quad (4.29)$$

The derivatives of the sediment transport rate in the x direction are:

$$\begin{aligned} \left. \frac{\partial q_{bxk}}{\partial h} \right|_0 &= \left. \frac{\partial q_{bk} \cos(\varphi_{sk})}{\partial h} \right|_0 = \cos(\varphi_{sk0}) \left. \frac{\partial q_{bk}}{\partial h} \right|_0 - q_{bk0} \sin(\varphi_{sk0}) \left. \frac{\partial \varphi_{sk}}{\partial h} \right|_0 = \\ &= \left. \frac{\partial q_{bk}}{\partial h} \right|_0 = \left. \frac{\partial q_{bk}}{\partial \theta_k} \right|_0 \left. \frac{\partial \theta_k}{\partial h} \right|_0 = \left. \frac{-q_{x0}}{h_0} \frac{\partial q_{bk}}{\partial q_x} \right|_0, \end{aligned} \quad (4.30)$$

$$\begin{aligned} \left. \frac{\partial q_{bxk}}{\partial q_x} \right|_0 &= \left. \frac{\partial q_{bk} \cos(\varphi_{sk})}{\partial q_x} \right|_0 = \cos(\varphi_{sk0}) \left. \frac{\partial q_{bk}}{\partial q_x} \right|_0 - q_{bk0} \sin(\varphi_{sk0}) \left. \frac{\partial \varphi_{sk}}{\partial q_x} \right|_0 = \\ &= \left. \frac{\partial q_{bk}}{\partial q_x} \right|_0, \end{aligned} \quad (4.31)$$

$$\begin{aligned} \left. \frac{\partial q_{bxk}}{\partial q_y} \right|_0 &= \left. \frac{\partial q_{bk} \cos(\varphi_{sk})}{\partial q_y} \right|_0 = \cos(\varphi_{sk0}) \left. \frac{\partial q_{bk}}{\partial q_y} \right|_0 - q_{bk0} \sin(\varphi_{sk0}) \left. \frac{\partial \varphi_{sk}}{\partial q_y} \right|_0 = \\ &= 0, \end{aligned} \quad (4.32)$$

$$\begin{aligned} \left. \frac{\partial q_{bxk}}{\partial M_{ak}} \right|_0 &= \left. \frac{\partial q_{bk} \cos(\varphi_{sk})}{\partial M_{ak}} \right|_0 = \cos(\varphi_{sk0}) \left. \frac{\partial q_{bk}}{\partial M_{ak}} \right|_0 - q_{bk0} \sin(\varphi_{sk0}) \left. \frac{\partial \varphi_{sk}}{\partial M_{ak}} \right|_0 = \\ &= \left. \frac{\partial q_{bk}}{\partial M_{ak}} \right|_0, \end{aligned} \quad (4.33)$$

$$\begin{aligned} \left. \frac{\partial q_{bxk}}{\partial \frac{\partial \eta}{\partial x}} \right|_0 &= \left. \frac{\partial q_{bk} \cos(\varphi_{sk})}{\partial \frac{\partial \eta}{\partial x}} \right|_0 = \cos(\varphi_{sk0}) \left. \frac{\partial q_{bk}}{\partial \frac{\partial \eta}{\partial x}} \right|_0 - q_{bk0} \sin(\varphi_{sk0}) \left. \frac{\partial \varphi_{sk}}{\partial \frac{\partial \eta}{\partial x}} \right|_0 = \\ &= 0, \end{aligned} \quad (4.34)$$

$$\begin{aligned} \left. \frac{\partial q_{bxk}}{\partial \frac{\partial \eta}{\partial y}} \right|_0 &= \left. \frac{\partial q_{bk} \cos(\varphi_{sk})}{\partial \frac{\partial \eta}{\partial y}} \right|_0 = \cos(\varphi_{sk0}) \left. \frac{\partial q_{bk}}{\partial \frac{\partial \eta}{\partial y}} \right|_0 - q_{bk0} \sin(\varphi_{sk0}) \left. \frac{\partial \varphi_{sk}}{\partial \frac{\partial \eta}{\partial y}} \right|_0 = \\ &= 0, \end{aligned} \quad (4.35)$$

where we have used that:

$$\cos(\varphi_{sk0}) = 1, \quad (4.36)$$

$$\sin(\varphi_{sk0}) = 0. \quad (4.37)$$

Note that:

$$\left. \frac{\partial q_{bk}}{\partial q_y} \right|_0 = \left. \frac{\partial q_{bk}}{\partial \theta_k} \right|_0 \left. \frac{\partial \theta_k}{\partial q_y} \right|_0 = 0, \quad (4.38)$$

and that the module of the sediment transport rate does not depend on the bed slope such that:

$$\left. \frac{\partial q_{bk}}{\partial \frac{\partial \eta}{\partial x}} \right|_0 = 0. \quad (4.39)$$

$$\left. \frac{\partial q_{bk}}{\partial \frac{\partial \eta}{\partial y}} \right|_0 = 0 . \quad (4.40)$$

We have related the derivative respect to the water depth to the derivative respect to the water discharge per unit width in the x direction:

$$\frac{\partial \theta_k}{\partial h} = \frac{-2C_f (q_x^2 + q_y^2)}{gRd_k h^3} , \quad (4.41)$$

$$\frac{\partial \theta_k}{\partial q_x} = \frac{2C_f q_x}{gRd_k h^2} , \quad (4.42)$$

$$\frac{\partial \theta_k}{\partial q_y} = \frac{2C_f q_y}{gRd_k h^2} , \quad (4.43)$$

which implies that:

$$\left. \frac{\partial \theta_k}{\partial h} \right|_0 = \frac{-q_{x0}}{h_0} \left. \frac{\partial \theta_k}{\partial q_x} \right|_0 , \quad (4.44)$$

$$\left. \frac{\partial \theta_k}{\partial q_y} \right|_0 = 0 . \quad (4.45)$$

The derivatives of the sediment transport rate in the y direction are:

$$\left. \frac{\partial q_{byk}}{\partial h} \right|_0 = \left. \frac{\partial q_{bk} \sin(\varphi_{sk})}{\partial h} \right|_0 = \sin(\varphi_{sk0}) \left. \frac{\partial q_{bk}}{\partial h} \right|_0 + q_{bk0} \cos(\varphi_{sk0}) \left. \frac{\partial \varphi_{sk}}{\partial h} \right|_0 = 0 \quad (4.46)$$

$$\left. \frac{\partial q_{byk}}{\partial q_x} \right|_0 = \left. \frac{\partial q_{bk} \sin(\varphi_{sk})}{\partial q_x} \right|_0 = \sin(\varphi_{sk0}) \left. \frac{\partial q_{bk}}{\partial q_x} \right|_0 + q_{bk0} \cos(\varphi_{sk0}) \left. \frac{\partial \varphi_{sk}}{\partial q_x} \right|_0 = 0 \quad (4.47)$$

$$\begin{aligned} \left. \frac{\partial q_{byk}}{\partial q_y} \right|_0 &= \left. \frac{\partial q_{bk} \sin(\varphi_{sk})}{\partial q_y} \right|_0 = \sin(\varphi_{sk0}) \left. \frac{\partial q_{bk}}{\partial q_y} \right|_0 + q_{bk0} \cos(\varphi_{sk0}) \left. \frac{\partial \varphi_{sk}}{\partial q_y} \right|_0 = \\ &= q_{bk0} \left. \frac{\partial \varphi_{sk}}{\partial q_y} \right|_0 = \frac{q_{bk0}}{q_{x0}} \left. \frac{\partial \varphi_{sk}}{\partial \varphi_\tau} \right|_0 \end{aligned} \quad (4.48)$$

$$\begin{aligned} \left. \frac{\partial q_{byk}}{\partial M_{ak}} \right|_0 &= \left. \frac{\partial q_{bk} \sin(\varphi_{sk})}{\partial M_{ak}} \right|_0 = \sin(\varphi_{sk0}) \left. \frac{\partial q_{bk}}{\partial M_{ak}} \right|_0 + q_{bk0} \cos(\varphi_{sk0}) \left. \frac{\partial \varphi_{sk}}{\partial M_{ak}} \right|_0 = \\ &= q_{bk0} \left. \frac{\partial \varphi_{sk}}{\partial M_{ak}} \right|_0 = 0 \end{aligned} \quad (4.49)$$

$$\left. \frac{\partial q_{byk}}{\partial \frac{\partial \eta}{\partial x}} \right|_0 = \left. \frac{\partial q_{bk} \sin(\varphi_{sk})}{\partial \frac{\partial \eta}{\partial x}} \right|_0 = \sin(\varphi_{sk0}) \left. \frac{\partial q_{bk}}{\partial \frac{\partial \eta}{\partial x}} \right|_0 + q_{bk0} \cos(\varphi_{sk0}) \left. \frac{\partial \varphi_{sk}}{\partial \frac{\partial \eta}{\partial x}} \right|_0 = 0 \quad (4.50)$$

$$\begin{aligned} \left. \frac{\partial q_{byk}}{\partial \frac{\partial \eta}{\partial y}} \right|_0 &= \left. \frac{\partial q_{bk} \sin(\varphi_{sk})}{\partial \frac{\partial \eta}{\partial y}} \right|_0 = \sin(\varphi_{sk0}) \left. \frac{\partial q_{bk}}{\partial \frac{\partial \eta}{\partial y}} \right|_0 + q_{bk0} \cos(\varphi_{sk0}) \left. \frac{\partial \varphi_{sk}}{\partial \frac{\partial \eta}{\partial y}} \right|_0 = \\ &= -\frac{q_{bk0}}{g_{sk0}} \left. \frac{\partial \varphi_{sk}}{\partial \varphi_{\tau}} \right|_0. \end{aligned} \quad (4.51)$$

Given that the angle of the sediment transport rate direction is small we write:

$$\varphi_{sk} \approx \tan(\varphi_{sk}) = \frac{\sin \varphi_{\tau} - \frac{1}{g_{sk}} \frac{\partial \eta}{\partial y}}{\cos \varphi_{\tau} - \frac{1}{g_{sk}} \frac{\partial \eta}{\partial x}} \approx \frac{\varphi_{\tau} - \frac{1}{g_{sk}} \frac{\partial \eta}{\partial y}}{1 - \frac{1}{g_{sk}} \frac{\partial \eta}{\partial x}}, \quad (4.52)$$

and:

$$\varphi_{\tau} \approx \tan(\varphi_{\tau}) = \frac{q_y - h\alpha_I \frac{q_x}{Q} I}{q_x - h\alpha_I \frac{q_y}{Q} I}. \quad (4.53)$$

We write:

$$\left. \frac{\partial \varphi_{sk}}{\partial h} \right|_0 = \left. \frac{\partial \varphi_{sk}}{\partial \varphi_{\tau}} \right|_0 \left. \frac{\partial \varphi_{\tau}}{\partial h} \right|_0, \quad (4.54)$$

$$\left. \frac{\partial \varphi_{sk}}{\partial q_x} \right|_0 = \left. \frac{\partial \varphi_{sk}}{\partial \varphi_{\tau}} \right|_0 \left. \frac{\partial \varphi_{\tau}}{\partial q_x} \right|_0, \quad (4.55)$$

$$\left. \frac{\partial \varphi_{sk}}{\partial q_y} \right|_0 = \left. \frac{\partial \varphi_{sk}}{\partial \varphi_{\tau}} \right|_0 \left. \frac{\partial \varphi_{\tau}}{\partial q_y} \right|_0. \quad (4.56)$$

$$\left. \frac{\partial \varphi_{sk}}{\partial \frac{\partial \eta}{\partial x}} \right|_0 = \left. \frac{\partial \varphi_{sk}}{\partial \varphi_{\tau}} \right|_0 \left. \frac{\partial \varphi_{\tau}}{\partial \frac{\partial \eta}{\partial x}} \right|_0. \quad (4.57)$$

$$\left. \frac{\partial \varphi_{sk}}{\partial \frac{\partial \eta}{\partial y}} \right|_0 = \left. \frac{\partial \varphi_{sk}}{\partial \varphi_{\tau}} \right|_0 \left. \frac{\partial \varphi_{\tau}}{\partial \frac{\partial \eta}{\partial y}} \right|_0. \quad (4.58)$$

where:

$$\left. \frac{\partial \varphi_{sk}}{\partial \varphi_{\tau}} \right|_0 = \frac{1}{1 - \frac{1}{g_{sk0}} \frac{\partial \eta}{\partial x}} \approx 1, \quad (4.59)$$

under the assumption that $\frac{\partial \eta}{\partial x} \ll 1$ and:

$$\left. \frac{\partial \varphi_\tau}{\partial h} \right|_0 = 0 \quad (4.60)$$

$$\left. \frac{\partial \varphi_\tau}{\partial q_x} \right|_0 = 0 \quad (4.61)$$

$$\left. \frac{\partial \varphi_\tau}{\partial q_y} \right|_0 = \frac{1}{q_{x0}} \quad (4.62)$$

$$\left. \frac{\partial \varphi_{sk}}{\partial \frac{\partial \eta}{\partial x}} \right|_0 = 0 \quad (4.63)$$

$$\left. \frac{\partial \varphi_{sk}}{\partial \frac{\partial \eta}{\partial y}} \right|_0 = \frac{-1}{g_{sk}} \quad (4.64)$$

The total derivative is:

$$\left. \frac{\partial q_{bx}}{\partial M_{ak}} \right|_0 = \sum_{k=1}^N \left. \frac{\partial q_{bxk}}{\partial M_{ak}} \right|_0 \quad (4.65)$$

$$\left. \frac{\partial q_{by}}{\partial \frac{\partial \eta}{\partial y}} \right|_0 = \sum_{k=1}^N \left. \frac{\partial q_{byk}}{\partial \frac{\partial \eta}{\partial y}} \right|_0 \quad (4.66)$$

4.5 Sediment Mass Conservation for each Grain Size in the Active Layer

The non-linear equation is:

$$\frac{\partial M_{ak}}{\partial t} - f_k^I \frac{\partial q_{bx}}{\partial x} - f_k^I \frac{\partial q_{by}}{\partial y} + \frac{\partial q_{bxk}}{\partial x} + \frac{\partial q_{byk}}{\partial y} = 0 \quad k \in \{1, N-1\} \quad (4.67)$$

Expanding the terms we obtain:

$$\begin{aligned} & \frac{\partial M_{ak}}{\partial t} + \left[\frac{\partial q_{bxk}}{\partial h} - f_k^I \frac{\partial q_{bx}}{\partial h} \right] \frac{\partial h}{\partial x} + \left[\frac{\partial q_{bxk}}{\partial q_x} - f_k^I \frac{\partial q_{bx}}{\partial q_x} \right] \frac{\partial q_x}{\partial x} + \\ & \left[\frac{\partial q_{bxk}}{\partial q_y} - f_k^I \frac{\partial q_{bx}}{\partial q_y} \right] \frac{\partial q_y}{\partial x} + \sum_{l=1}^{N-1} \left[\frac{\partial q_{bxk}}{\partial M_{al}} - f_k^I \frac{\partial q_{bx}}{\partial M_{al}} \right] \frac{\partial M_{al}}{\partial x} \\ & \left[\frac{\partial q_{bxk}}{\partial h} - f_k^I \frac{\partial q_{bx}}{\partial h} \right] \frac{\partial h}{\partial y} + \left[\frac{\partial q_{bxk}}{\partial q_x} - f_k^I \frac{\partial q_{bx}}{\partial q_x} \right] \frac{\partial q_x}{\partial y} + \\ & \left[\frac{\partial q_{bxk}}{\partial q_y} - f_k^I \frac{\partial q_{bx}}{\partial q_y} \right] \frac{\partial q_y}{\partial y} + \sum_{l=1}^{N-1} \left[\frac{\partial q_{bxk}}{\partial M_{al}} - f_k^I \frac{\partial q_{bx}}{\partial M_{al}} \right] \frac{\partial M_{al}}{\partial y} \\ & + \left[\frac{\partial q_{bxk}}{\partial \frac{\partial \eta}{\partial x}} - f_k^I \frac{\partial q_{bx}}{\partial \frac{\partial \eta}{\partial x}} \right] \frac{\partial^2 \eta}{\partial x^2} + \left[\frac{\partial q_{bxk}}{\partial \frac{\partial \eta}{\partial y}} - f_k^I \frac{\partial q_{bx}}{\partial \frac{\partial \eta}{\partial y}} \right] \frac{\partial^2 \eta}{\partial x \partial y} \\ & + \left[\frac{\partial q_{byk}}{\partial \frac{\partial \eta}{\partial x}} - f_k^I \frac{\partial q_{by}}{\partial \frac{\partial \eta}{\partial x}} \right] \frac{\partial^2 \eta}{\partial x \partial y} + \left[\frac{\partial q_{byk}}{\partial \frac{\partial \eta}{\partial y}} - f_k^I \frac{\partial q_{by}}{\partial \frac{\partial \eta}{\partial y}} \right] \frac{\partial^2 \eta}{\partial y^2} \end{aligned} \quad (4.68)$$

The linearized equation is:

$$\begin{aligned}
& \frac{\partial M'_{ak}}{\partial t} + \left[\frac{\partial q_{bxk}}{\partial h} \Big|_0 - f_{k0}^I \frac{\partial q_{bx}}{\partial h} \Big|_0 \right] \frac{\partial h'}{\partial x} + \left[\frac{\partial q_{bxk}}{\partial q_x} \Big|_0 - f_{k0}^I \frac{\partial q_{bx}}{\partial q_x} \Big|_0 \right] \frac{\partial q'_x}{\partial x} + \\
& \left[\frac{\partial q_{bxk}}{\partial q_y} \Big|_0 - f_{k0}^I \frac{\partial q_{bx}}{\partial q_y} \Big|_0 \right] \frac{\partial q'_y}{\partial x} + \sum_{l=1}^{N-1} \left[\frac{\partial q_{bxk}}{\partial M_{al}} \Big|_0 - f_{k0}^I \frac{\partial q_{bx}}{\partial M_{al}} \Big|_0 \right] \frac{\partial M'_{al}}{\partial x} \\
& \left[\frac{\partial q_{bxk}}{\partial h} \Big|_0 - f_{k0}^I \frac{\partial q_{bx}}{\partial h} \Big|_0 \right] \frac{\partial h'}{\partial y} + \left[\frac{\partial q_{bxk}}{\partial q_x} \Big|_0 - f_{k0}^I \frac{\partial q_{bx}}{\partial q_x} \Big|_0 \right] \frac{\partial q'_x}{\partial y} + \\
& \left[\frac{\partial q_{bxk}}{\partial q_y} \Big|_0 - f_{k0}^I \frac{\partial q_{bx}}{\partial q_y} \Big|_0 \right] \frac{\partial q'_y}{\partial y} + \sum_{l=1}^{N-1} \left[\frac{\partial q_{bxk}}{\partial M_{al}} \Big|_0 - f_{k0}^I \frac{\partial q_{bx}}{\partial M_{al}} \Big|_0 \right] \frac{\partial M'_{al}}{\partial y} \\
& + \left[\frac{\partial q_{bxk}}{\partial \frac{\partial \eta}{\partial x}} \Big|_0 - f_{k0}^I \frac{\partial q_{bx}}{\partial \frac{\partial \eta}{\partial x}} \Big|_0 \right] \frac{\partial^2 \eta'}{\partial x^2} + \left[\frac{\partial q_{bxk}}{\partial \frac{\partial \eta}{\partial y}} \Big|_0 - f_{k0}^I \frac{\partial q_{bx}}{\partial \frac{\partial \eta}{\partial y}} \Big|_0 \right] \frac{\partial^2 \eta'}{\partial x \partial y} \\
& + \left[\frac{\partial q_{byk}}{\partial \frac{\partial \eta}{\partial x}} \Big|_0 - f_{k0}^I \frac{\partial q_{by}}{\partial \frac{\partial \eta}{\partial x}} \Big|_0 \right] \frac{\partial^2 \eta'}{\partial x \partial y} + \left[\frac{\partial q_{byk}}{\partial \frac{\partial \eta}{\partial y}} \Big|_0 - f_{k0}^I \frac{\partial q_{by}}{\partial \frac{\partial \eta}{\partial y}} \Big|_0 \right] \frac{\partial^2 \eta'}{\partial y^2}
\end{aligned} \tag{4.69}$$

We have neglected the contribution of a perturbation to M_{ak} in f_k^I that would exist under aggradational conditions to avoid cases.

When considering the first regularization strategy based on a modification of the time scale of the mixing processes (Section 3.1), the only modification is that all terms in Equation ((4.68)) but the time derivative term are divided by α . When considering the second regularization strategy based on adding diffusion to the active layer equation (Section 3.2) two new terms are added to the left hand side of Equation ((4.68)):

$$-\kappa_{Hx} \frac{\partial^2 M'_{ak}}{\partial x^2} - \kappa_{Hy} \frac{\partial^2 M'_{ak}}{\partial y^2} . \tag{4.70}$$

5 Perturbation Analysis

In this section we conduct a perturbation analysis to study well-posedness of the system of equations. In Section 5.1 we write the linear model in matrix-vector formulation, as it is convenient to analyze the system of equations. In Section 5.2 we obtain the eigenvalue problem of the linear model. In Section 5.3 we define the concept of ill-posedness based on the eigenvalue problem of the linear model.

5.1 Matrix Formulation

In this section we write the system of equations in matrix formulation. The equation for the mass conservation of sediment in the substrate (Equation ((2.11))) is a linear combination of the active layer equation (Eq. (2.10)) and the *Exner* equation (Eq. (2.9)). The rest of the equations do not depend on M_{sk} . Thus, the substrate equations provide a zero eigenvalue with multiplicity $N - 1$. To simplify the writing we omit the substrate equations.

We recast the system of perturbed equations, ((4.8)), ((4.12)), ((4.23)), ((4.29)), and ((4.69)) in matrix form:

$$\frac{\partial \mathbf{Q}'}{\partial t} + \mathbf{D}_{x0} \frac{\partial^2 \mathbf{Q}'}{\partial x^2} + \mathbf{D}_y \frac{\partial^2 \mathbf{Q}'}{\partial y^2} + \mathbf{C}_0 \frac{\partial^2 \mathbf{Q}'}{\partial x \partial y} + \mathbf{A}_{x0} \frac{\partial \mathbf{Q}'}{\partial x} + \mathbf{A}_{y0} \frac{\partial \mathbf{Q}'}{\partial y} + \mathbf{B}_0 \mathbf{Q}' = 0 \quad (5.1)$$

The vector of dependent variables is:

$$\mathbf{Q}' = \begin{bmatrix} h' \\ q'_x \\ q'_y \\ \eta' \\ [M'_{ak}] \end{bmatrix} \quad (5.2)$$

The diffusive matrix in x direction is:

$$\mathbf{D}_{x0} = \mathbf{0} \quad (5.3)$$

The diffusive matrix in y direction is:

$$\mathbf{D}_{y0} = \begin{bmatrix} 0 & 0 & 0 & 0 & 0 & 0 \\ 0 & 0 & 0 & 0 & 0 & 0 \\ 0 & 0 & 0 & 0 & 0 & 0 \\ 0 & 0 & 0 & \frac{\partial q_{by}}{\partial \frac{\partial \eta}{\partial y}} \Big|_0 & 0 & 0 \\ \hline 0 & 0 & 0 & \left[\frac{\partial q_{byk}}{\partial \frac{\partial \eta}{\partial y}} \Big|_0 \quad - \int_{k0}^I \frac{\partial q_{by}}{\partial \frac{\partial \eta}{\partial y}} \Big|_0 \right] & 0 & 0 \end{bmatrix} \quad (5.4)$$

The matrix of cross derivatives is:

$$\mathbf{C}_0 = \mathbf{0} \quad (5.5)$$

The system matrix in x direction is:

$$\mathbf{A}_{x0} = \begin{bmatrix} 0 & 1 & 0 & 0 & 0 \\ gh_0 - \left(\frac{q_{x0}}{h_0}\right)^2 & 2\frac{q_{x0}}{h_0} & 0 & gh_0 & 0 \\ 0 & 0 & \frac{q_{x0}}{h_0} & 0 & 0 \\ \left.\frac{\partial q_{bx}}{\partial h}\right|_0 & \left.\frac{\partial q_{bx}}{\partial q_x}\right|_0 & 0 & 0 & \left[\frac{\partial q_{bx}}{\partial M_{al}}\right]_0 \\ \left[\frac{\partial q_{bxk}}{\partial h}\right]_0 - f_{k0}^I \left.\frac{\partial q_{bx}}{\partial h}\right|_0 & \left[\frac{\partial q_{bxk}}{\partial q_x}\right]_0 - f_{k0}^I \left.\frac{\partial q_{bx}}{\partial q_x}\right|_0 & 0 & 0 & \left[\frac{\partial q_{bxk}}{\partial M_{al}}\right]_0 - f_{k0}^I \left.\frac{\partial q_{bx}}{\partial M_{al}}\right|_0 \end{bmatrix} \quad (5.6)$$

The system matrix in y direction is:

$$\mathbf{A}_{y0} = \begin{bmatrix} 0 & 0 & 1 & 0 & 0 \\ 0 & 0 & \frac{q_{x0}}{h_0} & 0 & 0 \\ gh_0 & 0 & 0 & gh_0 & 0 \\ 0 & 0 & \left.\frac{\partial q_{by}}{\partial q_y}\right|_0 & 0 & 0 \\ 0 & 0 & \left[\frac{\partial q_{byk}}{\partial q_y}\right]_0 - f_{k0}^I \left.\frac{\partial q_{by}}{\partial q_y}\right|_0 & 0 & 0 \end{bmatrix} \quad (5.7)$$

The matrix of linear terms is:

$$\mathbf{B}_0 = \begin{bmatrix} 0 & 0 & 0 & 0 & 0 \\ \frac{-3C_f q_{x0}^2}{h_0^3} & \frac{2C_f q_{x0}}{h_0^2} & 0 & 0 & 0 \\ 0 & 0 & \frac{C_f q_{x0}}{h_0^2} & 0 & 0 \\ 0 & 0 & 0 & 0 & 0 \\ 0 & 0 & 0 & 0 & 0 \end{bmatrix} \quad (5.8)$$

Note that the only derivatives that need to be computed are (see Section 4.4):

$$\frac{\partial q_{bk}}{\partial q_x} \forall k \quad \text{and} \quad \frac{\partial q_{bk}}{\partial M_{al}} \forall k, \quad l \in [1, N-1]. \quad (5.9)$$

Considering that hiding is not a function of the flow discharge, we write:

$$\frac{\partial q_{bk}}{\partial q_x} = \frac{\partial q_{bk}}{\partial \theta_k} \frac{\partial \theta_k}{\partial q_x} = F_{ak} \frac{\sqrt{gRd_k^3}}{(1-p)} \frac{2C_f q_x}{gRd_k h^2} \frac{\partial q_{bk}^*}{\partial \theta_k} \quad (5.10)$$

Furthermore we expand the second derivative of Equation ((5.9)) as:

$$\frac{\partial q_{bk}}{\partial M_{al}} = \frac{\sqrt{gRd_k^3}}{(1-p) L_a} \left(q_{bk}^* \frac{\partial F_{ak}}{\partial F_{al}} + F_{ak} \frac{\partial q_{bk}^*}{\partial F_{al}} \right) \quad (5.11)$$

The first term of the right hand side in equation (5.11) is:

$$\frac{\partial F_{ak}}{\partial F_{al}} = \begin{cases} 1 & \text{for } k = l, 1 \leq (k, l) < N-1, \\ 0 & \text{for } k \neq l, 1 \leq (k, l) < N-1, \\ -1 & \text{for } k = N, \forall l \end{cases} \quad (5.12)$$

Note that we account for the constrain in Equation ((2.12)). The second term of the right hand side in Equation ((5.11)) is related to hiding and is expanded as:

$$\frac{\partial q_{bk}^*}{\partial F_{al}} = \frac{\partial q_{bk}^*}{\partial \xi_k} \frac{\partial \xi_k}{\partial F_{al}} = \frac{\partial q_{bk}^*}{\partial \xi_k} \frac{\partial \xi_k}{\partial D_m} \frac{\partial D_m}{\partial F_{al}}, \quad (5.13)$$

where we assume that the hiding function depends on the volume fraction content of sediment in the active layer through the mean grain size. Thus, all terms in the matrices depend on the following derivatives only:

$$\frac{\partial q_{bk}^*}{\partial \theta_k} \forall k, \frac{\partial q_{bk}^*}{\partial \xi_k} \forall k, \frac{\partial \xi_k}{\partial D_m} \forall k, \quad \text{and} \quad \frac{\partial D_m}{\partial F_{al}} \quad l \in [1, N - 1]. \quad (5.14)$$

In this manner, given independent closure relations for the nondimensional sediment transport rate, hiding, and mean grain size, one obtains all the derivatives to build the matrices. In Appendix A we compute the derivatives for some closure relations.

When applying the first regularization strategy (Section 3.1), the terms from the 5th row until the end and in all columns are divided by α . When applying the second regularization strategy (Section 3.2), the lower right submatrix of matrices \mathbf{D}_x and \mathbf{D}_y have an additional term in the main diagonal equal to $-\kappa_{Hx}$ and $-\kappa_{Hy}$, respectively.

5.2 Eigenvalue Problem

We assume that the perturbations can be represented as a Fourier series, which implies that they are piecewise smooth and bounded for $x = \pm\infty$. Using this assumption the solution of the perturbed system is expressed in the form of normal modes:

$$\mathbf{Q}' = \text{Re} \left(\mathbf{V} e^{i(k_{wx} + k_{wy} - \omega t)} \right), \quad (5.15)$$

where i is the imaginary unit, k_{wx} [rad/m] and k_{wy} [rad/m] are the real wave numbers in x and y direction, respectively, $\omega = \omega_r + i\omega_i$ [rad/s] is the complex angular frequency, \mathbf{V} is the complex amplitude vector, and Re denotes the real part of the solution (which we will omit in the subsequent steps). The variable ω_r is the angular frequency and ω_i the attenuation coefficient. A value of $\omega_i > 0$ implies growth of perturbations and $\omega_i < 0$ decay. Substitution of equation ((5.15)) in equation ((5.1)) yields:

$$[\mathbf{M}_0 - \omega \mathbf{1}] \mathbf{V} = 0, \quad (5.16)$$

where:

$$\mathbf{M}_0 = \mathbf{D}_{x0} k_{wx}^2 \mathbf{i} + \mathbf{D}_{y0} k_{wy}^2 \mathbf{i} + \mathbf{A}_{x0} k_{wx} + \mathbf{A}_{y0} k_{wy} - \mathbf{B}_0 \mathbf{i}, \quad (5.17)$$

and $\mathbf{1}$ denotes the unit matrix. Equation ((5.16)) is an eigenvalue problem in which the eigenvalues of \mathbf{M}_0 (as a function of the wave number) are the values of ω satisfying equation ((5.16)).

The solution of the linear model provides information regarding the development of small amplitude oscillations only, but for an arbitrary wave number. For this reason the linear model is convenient for studying the well-posedness of the model, which we will assess subsequently.

5.3 Instability, Hyperbolicity, and Ill-Posedness

Ill-posedness has been related to the system of governing equations losing its hyperbolic character. Stability analysis investigates growth and decay of perturbations of a base state. The two mathematical problems may seem unrelated but in fact they are strongly linked. In this section we clarify the terms unstable, hyperbolic, and ill-posed, and present the mathematical framework that we use to study the well-posedness of the system of equations.

A system is stable if perturbations to an equilibrium state decay and the solution returns to its original state. This is equivalent to saying that all possible combinations of wave numbers in the x and y directions yield a negative growth rate (ω_i , equation ((5.15))). An example of a stable system in hydrodynamics is the inviscid Shallow Water Equations (iSWE) for a Froude number smaller than 2 (*Jeffreys, 1925; Balmforth and Mandre, 2004; Colombini and Stocchino, 2005*). In figure 5.1a we show the maximum growth rate of perturbations to a reference solution (Case I1, tables 5.1 and 5.2) of the iSWE on an inclined plane (i.e., the first 3 equations of the complete system, equation ((5.1)), with neither secondary flow nor diffusion). The growth rate is obtained numerically by computing the eigenvalues of the reduced matrix \mathbf{M}_0 (the first 3 rows and columns in equation ((5.17))) for wave numbers between 0 and 250 rad/m, which is equivalent to wavelengths ($l_{wx} = 2\pi/k_{wx}$ and equivalently for y) down to 1 cm. Figure 5.1b presents the same information as figure 5.1a in terms of wavelength rather than wave number to better illustrate the behaviour for large wavelengths. The growth rate is negative for all wave numbers, which confirms that the iSWE for $Fr < 2$ yield a stable solution.

u [m/s]	v [m/s]	h [m]	C_f [-]
1	0	1	0.007

Table 5.1: Reference state.

Case	model	Fr	stability	mathematical character
I1	iSWE	0.32	stable	well-posed
B1	iSWE+Exner	0.32	unstable	well-posed
I2	iSWE	2.01	unstable	ill-posed

Table 5.2: Cases of a stable well-posed model (I1), an unstable well-posed model (B1), and an ill-posed model (I2). Case I2 has the same parameter values as Case I1 but for the mean flow velocity which is equal to 6.30 m/s.

A system is unstable when perturbations to an equilibrium state grow and the solution diverges from the initial equilibrium state. The growth of river bars is an example of an unstable system in river morphodynamics. A straight alluvial channel is stable if the width-to-depth ratio is sufficiently small and, above a certain threshold value, the channel becomes unstable and free alternate bars grow (*Engelund and Skovgaard, 1973; Fredsøe, 1978; Colombini et al., 1987; Schielen et al., 1993*). Mathematically, an unstable system has a region, a domain in the wave number space, in which the growth rate of perturbations is positive. In figure 5.1c-d we present the growth rate of perturbations to a reference solution consisting of uniform flow (table 5.1) on an alluvial bed composed of unisize sediment with a characteristic grain size equal to 0.001 m (Case B1, table 5.2). The sediment transport rate is computed using the relation by *Engelund and Hansen (1967)* and the effect of the bed slope on the sediment transport direction is accounted for using the simplest formulation, $g_s = 1$. Figure 5.1d confirms the classical result of linear bar theory: there exists a critical transverse wavelength (l_{wyc}) below which all perturbations decay. In our particular case $l_{wyc} = 40.2 m$. Impermeable boundary conditions at the river banks limit the possible wavelengths to fractions of the channel width B

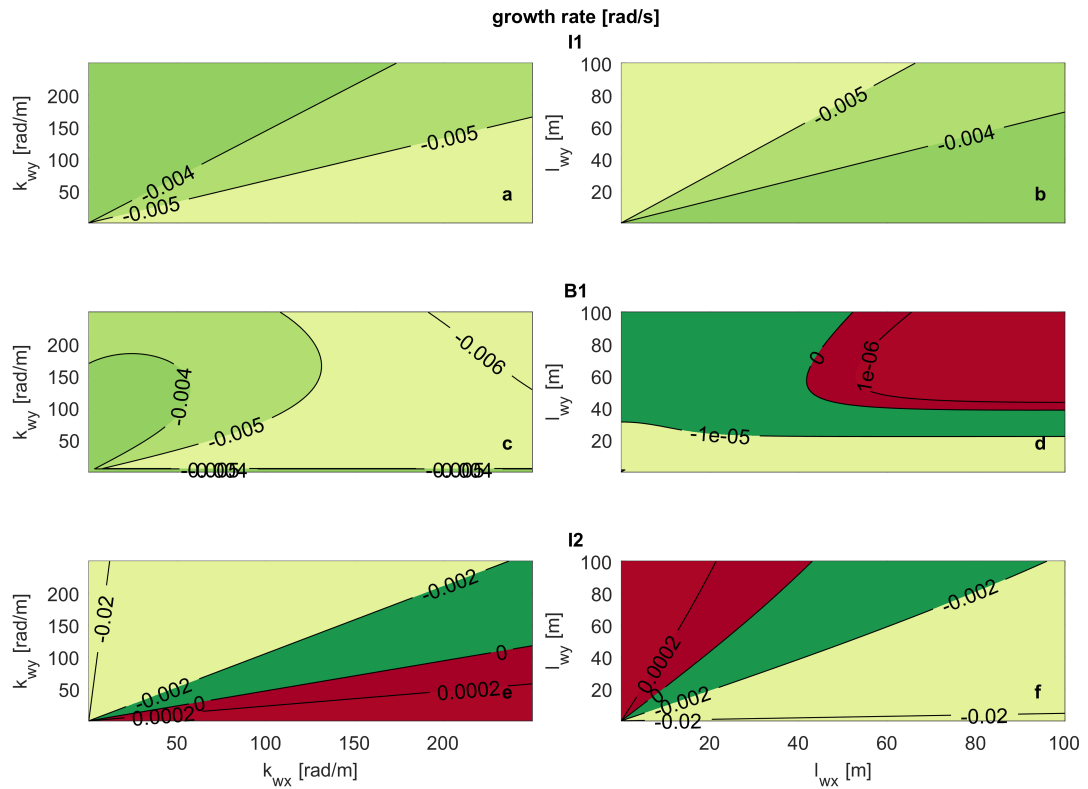


Figure 5.1: Growth rate of perturbations added to the reference case (tables 5.1 and 5.2) as a function of the wave number and the wavelength: (a)-(b) iSWE, $Fr < 2$ (Case I1, well-posed), (c)-(d) iSHE+Exner (Case B1, well-posed), and (e)-(f) iSWE, $Fr > 2$ (Case I2, ill-posed). The subplots in the two columns show the same information but highlight the behaviour for large wave numbers (left column) and for large wavelengths (right column). Red and green indicates growth and decay of perturbations, respectively.

[m] such that $l_{wy} = 2B/m$ for $m = 1, 2, \dots$ (Callander, 1969). As the most unstable mode is the first one (i.e., $m = 1$, alternate bars) (Colombini et al., 1987; Schielen et al., 1993), the minimum channel width above which perturbations grow is $B_c = l_{wyc}/2 = 20.1 m$, which confirms the results of Schielen et al. (1993). Figure 5.1c highlights, as for case I1, the decay of short waves.

A particular case of instability is that in which the domain of positive growth rate extends to infinitely large wave numbers (i.e., short waves). Under this condition there is no cutoff wave number above which we can neglect the contribution of ever shorter waves with non-zero growth rates. For any unstable perturbation a shorter one can be found which is even more unstable. This implies that the growth rate of an infinitesimal perturbation (i.e., noise) tends to infinity. Such a system cannot represent a physical phenomenon, as the growth rate of any physical process in nature is bounded. A system in which the growth rate of infinitesimal perturbations tends to infinity does not have a unique solution depending continuously on the initial and boundary conditions, which implies that the system is ill-posed (Hadamard, 1923; Joseph and Saut, 1990). An example of an ill-posed hydrodynamic model is the iSWE for flow with a Froude number larger than 2. In figure 5.1e-f we show the growth rate of perturbations to the reference solution of a case in which the Froude number is slightly larger than 2 (Case I2, table 5.2). The growth rate extends to infinitely large wave numbers, which confirms that this case is ill-posed. A model being ill-posed is an indication that there is a

relevant physical mechanism that has been neglected in the model derivation (Fowler, 1997). Viscous forces regularise the iSWE (i.e., make the model well-posed) and rather than ill-posed, the viscous Shallow Water Equations become simply unstable for a Froude number larger than 2, predicting the formation of roll-waves (Balmforth and Mandre, 2004; Balmforth and Vakil, 2012; Rodrigues and Zumbrun, 2016; Barker et al., 2017a,b).

Chaotic models, just as ill-posed models, are sensitive to the initial and boundary conditions and lose their predictive capabilities in a deterministic sense (Lorenz, 1963). Yet, there are two essential differences. First, chaotic systems lose their predictive capabilities after a certain time (Devaney, 1989; Banks et al., 1992), yet there exists a finite time in which the dynamics are predictable. In ill-posed models infinitesimal perturbations to the initial condition cause a finite divergence in the solution in an arbitrarily (but fixed) short time. Second, while the dynamics of a chaotic model are not predictable in deterministic terms after a certain time, these continue to be predictable in statistical terms. For this reason, although being sensitive to the initial and boundary conditions, a model presenting chaotic properties can be used, for instance, to capture the essential dynamics and spatio-temporal features of river braiding (Murray and Paola, 1994, 1997). On the contrary, the dynamics of an ill-posed model cannot be analysed in statistical terms.

The numerical solution of an ill-posed problem continues to change as the grid is refined because a smaller grid size resolves larger wave numbers with faster growth rates (Joseph and Saut, 1990; Kabanikhin, 2008; Barker et al., 2015; Woodhouse et al., 2012). In other words, the numerical solution of an ill-posed problem does not converge when the grid cell size is reduced. This property emphasizes the unrealistic nature of ill-posed problems and shows that ill-posed models cannot be applied in practice.

We present an example of grid dependence specifically related to river morphodynamics under conditions with mixed-size sediment. We consider a case of degradation into a substrate finer than the active layer, as this is a situation in which the active layer model is prone to be ill-posed (Section 1). The reference state is the same as in Case B1, yet the sediment is a mixture of two sizes equal to 0.001 m and 0.010 m. The bed surface is composed of 10 % of fine sediment. The active layer thickness is equal to 0.05 m, which in this case is representative of small dunes covering the bed (e.g. Deigaard and Fredsøe, 1978; Armanini and Di Silvio, 1988; Blom, 2008). Depending on the substrate composition, this situation yields an ill-posed model (Chavarrías et al., 2018). When the substrate is composed of 50 % of fine sediment (Case H1, table 5.3), the problem is well-posed and it is ill-posed when the substrate is composed of 90 % of fine sediment (Case H2, table 5.3).

We use the software package Delft3D-4 (Lesser et al., 2004) to solve the system of equations. We stress that the problem of ill-posedness is inherent to the system of equations and independent from the numerical solver. We have implemented a subroutine that assesses the well-posedness of the system of equations at each node and time step. The domain is 100 m long and 10 m wide. The downstream water level is lowered at a rate of 0.01 m/h to induce degradational conditions. The upstream sediment load is constant and equal to the equilibrium value of the reference state (Blom et al., 2017). The cells are square and we consider three different sizes (table 5.3). The time step varies between simulations to maintain a constant value of the CFL number.

Figure 5.2 presents the bed elevation after 10 h. The result of the well-posed case (H1, left column) is grid independent. The result of the ill-posed case (H2, right column) changes as the grid is refined and presents an oscillatory pattern characteristic of ill-posed simulations (Joseph and Saut, 1990; Woodhouse et al., 2012; Barker et al., 2015; Chavarrías et al., 2018). The bed seems to be flat in the ill-posed simulation with a coarser grid (figure 5.2b). This is

Case	f_1^I [-]	Δx [m]	mathematical character
H1a	0.5	0.50	well-posed
H1b	0.5	0.25	well-posed
H1c	0.5	0.10	well-posed
H2a	0.9	0.50	ill-posed
H2b	0.9	0.25	ill-posed
H2c	0.9	0.10	ill-posed

Table 5.3: Cases showing the effect of grid cell size on the numerical solution of well-posed and ill-posed models.

because oscillations grow slowly on a coarse grid and require more time to be perceptible. The waviness of the bed is seen in the result of the check routine, as it predicts ill-posedness only at those locations where the bed degrades (the stoss face of the oscillations). The fact that the model is well-posed in almost the entire domain in the ill-posed case solved using a cell sizes equal to 0.25 m (H2b, figure 5.2d) and 0.10 m (H2c, figure 5.2f) does not mean that the results are realistic. Non-physical oscillations have grown and vertically mixed the sediment such that the situation is well-posed after 10 h (Chavarrías *et al.*, 2018). We provide a movie of figure 5.2 in the online supplementary material.

In the above idealised situations it is evident that the oscillations are non-physical and it is straightforward to do a converge test to clarify that the solution is grid dependent. In complex domains in which several processes play a role, it is more difficult to associate oscillations to ill-posedness. Moreover, in long term applications the growth rate of perturbations may be fast compared to the frequency at which model results are assessed, which may hide the consequences of ill-posedness. If one studies a process that covers months or years (and consequently analyses the results on a monthly basis) but perturbations due to ill-posedness grow on an hourly scale, it may be difficult to identify that the problem is ill-posed. Using poor numerical techniques to solve the system of equations also contributes to hiding the consequences of ill-posedness as numerical diffusion dampens perturbations. These factors may explain why the problem of ill-posedness in mixed-sediment river morphodynamics is not widely acknowledged.

In the river morphodynamics community, the term ellipticity has been used to refer to ill-posedness of the system of equations in contrast to hyperbolicity, which is associated to well-posedness (Ribberink, 1987; Mosselman, 2005; Stecca *et al.*, 2014; Siviglia *et al.*, 2017; Chavarrías *et al.*, 2018). In general the terms are equivalent, but not always. We consider a unit vector \hat{n} in the direction (x, y) , $\hat{n} = (\hat{n}_x, \hat{n}_y)$. The system of equations ((5.1)) is hyperbolic if matrix $\mathbf{A} = \mathbf{A}_{x0}\hat{n}_x + \mathbf{A}_{y0}\hat{n}_y$ diagonalises with real eigenvalues $\forall \hat{n}$ (e.g. LeVeque, 2004; Castro *et al.*, 2009). Neglecting friction and diffusive processes (i.e., $\mathbf{B}_0 = \mathbf{D}_{x0} = \mathbf{D}_{y0} = \mathbb{0}$), hyperbolicity implies that the eigenvalues of \mathbf{M}_0 (equation ((5.17))) are real. In this case, as the growth rate of perturbations (i.e., the imaginary part of the eigenvalues of \mathbf{M}_0) is equal to 0 regardless of the wave number, the system of equations is well-posed. As the coefficients of \mathbf{A} are real, complex eigenvalues appear in conjugate pairs. This means that if \mathbf{A} has a complex eigenvalue (i.e., the problem is not hyperbolic), at least one wave will have a positive growth rate. Neglecting friction and diffusive processes, non-hyperbolicity implies that infinitely large wave numbers have a positive growth rate. We conclude that, in the absence of diffusion and friction, lack of hyperbolicity implies ill-posedness. Note that ellipticity (i.e., the eigenvalues of \mathbf{A} are all complex) is not required for the problem to be ill-posed, as it suffices that the problem is not hyperbolic. When considering diffusion and friction even when \mathbf{A} has complex eigenvalues, the imaginary part of the eigenvalues of \mathbf{M}_0 may all be

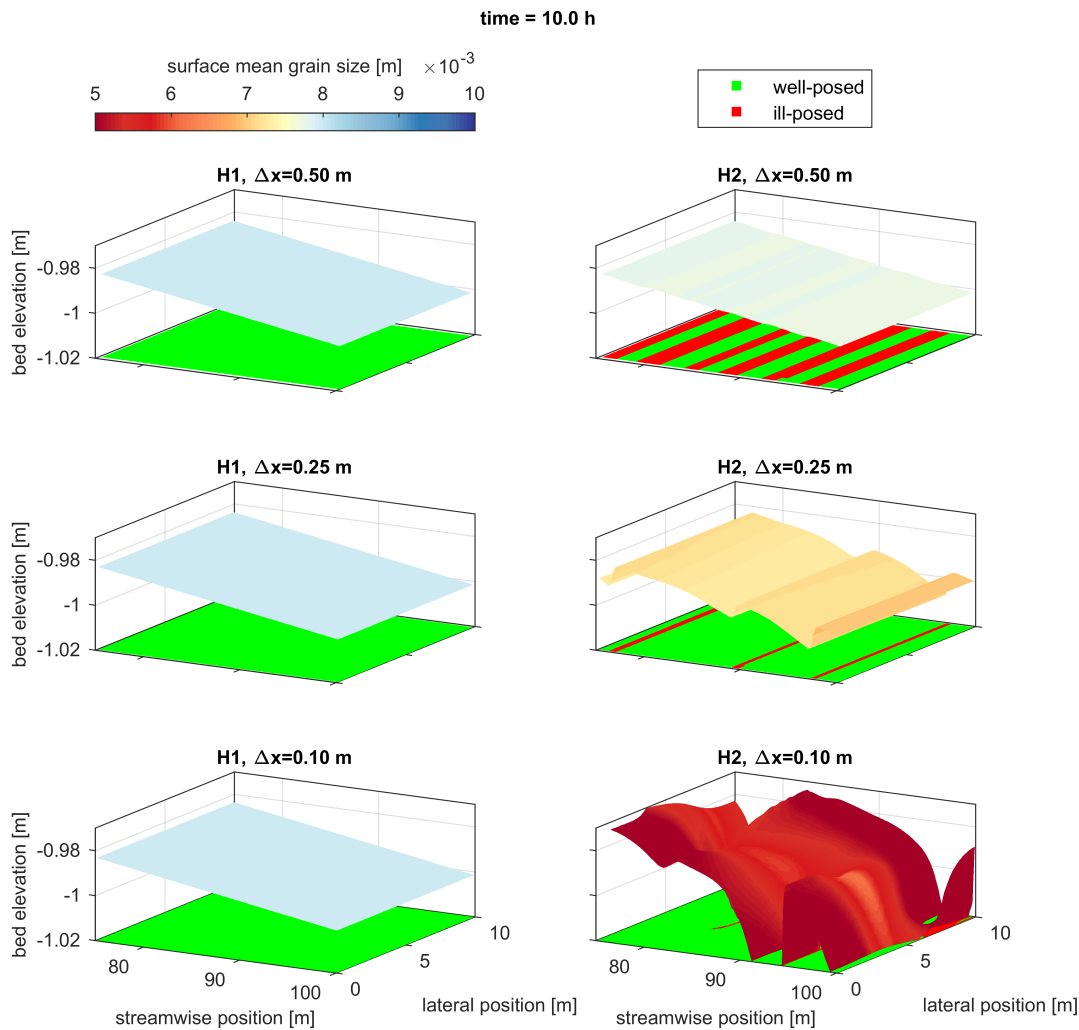


Figure 5.2: Simulated bed elevation (surface) and mean grain size at the bed surface (colour) of a well-posed case (left column, H1, table 5.3) and an ill-posed case (right column, H2, table 5.3). In each row we present the results for varying cell size. The colour of the $x - y$ plane shows the result of the routine that checks whether the conditions at each node yield a well-posed (green) or an ill-posed (red) model.

negative and the problem well-posed.

Finally, well-posedness and hyperbolicity are similar terms when dealing with problems arising from conservation laws and changes with time, as hyperbolicity guarantees the existence of wave solutions (Lax, 1980; Courant and Hilbert, 1989; Strikwerda, 2004; Toro, 2009; Dafermos, 2010; Bressan, 2011; Dafermos, 2016). In communities such as materials science, it is the term hyperbolicity that is associated to ill-posedness, as a smooth solution of, for instance the stress, requires that the system is elliptic (Knowles and Sternberg, 1975, 1976; Veprek et al., 2007).

6 Analytical Results

In this section we analytically study the properties of the regularization strategies. To this end, we simplify the system of equations by considering two sediment size fractions only (Section 6.1). Moreover, we assume that the Froude number is sufficiently small such that it is reasonable to assume that changes in flow are orders of magnitude faster than morphodynamic changes (i.e., quasi-steady flow assumption (*De Vries, 1965; Cao and Carling, 2002; Colom-bini and Stocchino, 2005*)). Finally, we assume that the active layer thickness is constant. In Section 6.2 we describe the procedure to test for ill-posedness. We report the results of the regularization strategy consisting of a modification of the time scale of mixing-processes (Section 6.3) and of including diffusion in the active layer equation (Section 6.4).

6.1 Two Sediment Size Fractions Model

In this section we write the model for two sediment size fractions. We use the notation introduced by *Chavarrías et al. (2019a)*. Subscripts k and l refer to the grain size fraction while the subscript j refers to the direction (i.e., x and y). The parameters are a generalization of the parameters used by *Stecca et al. (2014)* and *Chavarrías et al. (2018)* to the x and y direction.

Parameter $\psi_j [-]$ represents the sediment transport intensity (e.g. *De Vries, 1965; Lyn and Altinakar, 2002; Stecca et al., 2014*) and ranges between 0 (no sediment transport) and $\mathcal{O}(10^{-2})$ (high sediment discharge):

$$\psi_j = \frac{\partial q_{bj}}{\partial q_j} . \quad (6.1)$$

Parameter $c_{jk} \in [0, 1] [-]$ represents the sediment transport intensity of fraction k relative to the total sediment transport intensity:

$$c_{jk} = \frac{1}{\psi_j} \frac{\partial q_{bjk}}{\partial q_j} . \quad (6.2)$$

Parameter $\gamma_{jk} [-]$ represents the sediment transport intensity of fraction k relative to the fraction content of sediment of fraction k at the interface between the active layer and the substrate:

$$\gamma_{jk} = c_{jk} - f_k^I , \quad (6.3)$$

Parameter $\chi_{jk} [-]$ represents the nondimensional rate of change of the total sediment transport rate with respect to the change of volume of sediment of size fraction k in the active layer:

$$\chi_{jk} = \frac{1}{u_j} \frac{\partial q_{bj}}{\partial M_{ak}} . \quad (6.4)$$

Parameter $d_{jk,l} [-]$ represents the nondimensional rate of change of the sediment transport rate of size fraction l with respect to the volume of sediment of size fraction k in the active layer:

$$d_{jk,l} = \frac{1}{u_j \chi_{jk}} \frac{\partial q_{bjl}}{\partial M_{ak}} . \quad (6.5)$$

Parameter $\mu_{jk,l} [-]$ represents the rate of change of the sediment transport rate with respect to the volume of sediment in the active layer relative to the fraction content of sediment of fraction k at the interface between the active layer and the substrate:

$$\mu_{jk,l} = d_{jk,l} - f_k^I . \quad (6.6)$$

Parameter $R_j < 0$ [m²/s] represents the effect of the bed slope on the direction of the sediment transport rate:

$$R_j = \frac{\partial q_{bj}}{\partial s_j}, \quad (6.7)$$

where $s_j = \partial\eta/\partial j$. Parameter r_{jk} [–] represents the effect of the bed slope on the direction of the sediment transport rate of fraction k relative to the total effect:

$$r_{jk} = \frac{1}{R_j} \frac{\partial q_{bjk}}{\partial s_j}. \quad (6.8)$$

Parameter l_{jk} [–] represents the effect of the bed slope on the direction of the sediment transport rate of fraction k relative to the fraction content of sediment at the interface between the active layer and the substrate:

$$l_{jk} = r_{jk} - f_k^I. \quad (6.9)$$

Using this notation, the diffusive matrix in y direction considering two sediment size fractions is:

$$\mathbf{D}_{y0} = \begin{bmatrix} 0 & 0 & 0 & 0 & 0 \\ 0 & 0 & 0 & 0 & 0 \\ 0 & 0 & 0 & 0 & 0 \\ 0 & 0 & 0 & R_y & 0 \\ 0 & 0 & 0 & R_y l_{y1} & 0 \end{bmatrix} \quad (6.10)$$

The system matrix in x direction is:

$$\mathbf{A}_{x0} = \begin{bmatrix} 0 & 1 & 0 & 0 & 0 \\ u^2 \left(\frac{1}{Fr^2} - 1 \right) & 2u & 0 & \frac{u^2}{Fr^2} & 0 \\ 0 & 0 & u & 0 & 0 \\ -u\psi_x & \psi_x & 0 & 0 & u\chi_{x1} \\ -u\psi_x\gamma_{x1} & \psi_x\gamma_{x1} & 0 & 0 & u\chi_{x1}\mu_{x1,1} \end{bmatrix} \quad (6.11)$$

The system matrix in y direction is:

$$\mathbf{A}_{y0} = \begin{bmatrix} 0 & 0 & 1 & 0 & 0 \\ 0 & 0 & u & 0 & 0 \\ \frac{u^2}{Fr^2} & 0 & 0 & \frac{u^2}{Fr^2} & 0 \\ 0 & 0 & \psi_y & 0 & 0 \\ 0 & 0 & \psi_y\gamma_{y1} & 0 & 0 \end{bmatrix} \quad (6.12)$$

We have omitted the subscript 0 to facilitate reading.

6.2 Ill-posedness Test

In this section we study under which conditions the model accounting for two sediment size fractions is ill-posed. To this end, we study the sign of the imaginary part of the eigenvalues of the model as the wavenumbers tends to infinity. In order to obtain analytical solutions, apart from considering two sediment size fractions, we consider quasi-steady flow. Under these conditions, the model has two eigenvalues only. The eigenvalues ω of the model are found as the roots of the characteristic polynomial:

$$\mathbf{R} = \begin{bmatrix} 0 & 0 & 0 & 0 & 0 \\ 0 & 0 & 0 & 0 & 0 \\ 0 & 0 & 0 & 0 & 0 \\ 0 & 0 & 0 & \omega & 0 \\ 0 & 0 & 0 & 0 & \omega \end{bmatrix} - \mathbf{M}_0 \quad (6.13)$$

We consider three cases in which the wavenumber tends to infinity:

- 1 $k_{wx} = k_{wy} \rightarrow \text{inf}$,
- 2 $k_{wx} = 0$ and $k_{wy} \rightarrow \text{inf}$,
- 3 $k_{wx} \rightarrow \text{inf}$ and $k_{wy} = 0$.

In Case 1, the maximum imaginary part of the two eigenvalues is equal to:

$$\omega_i^{\text{lim}} = \frac{C_{fg}}{u} \chi_{x1} (r_{y1} - d_{x1,1}) \frac{\text{Fr}^2 (4\text{Fr}^2 - 3)}{\text{Fr}^2 - 2} + \omega_{\text{if}}^{\text{lim}}, \quad (6.14)$$

where $\omega_{\text{if}}^{\text{lim}}$ [rad/s] is the maximum imaginary part of the eigenvalues neglecting the effect of friction as found by [Chavarrías et al. \(2019a\)](#):

$$\omega_{\text{if}}^{\text{lim}} = \frac{-u^2 \chi_{x1}}{R_y} [\chi_{x1} l_{y1} (r_{y1} - d_{x1,1}) + e_x^{\text{lim}} (r_{y1} - c_{x1}) + e_y^{\text{lim}} (r_{y1} - c_{y1})] \quad (6.15)$$

where:

$$e_x^{\text{lim}} = \frac{\psi_x}{2 - \text{Fr}^2}, \quad (6.16)$$

$$e_y^{\text{lim}} = \frac{\psi_y}{2 - \text{Fr}^2}. \quad (6.17)$$

The order of magnitude of $\omega_{\text{if}}^{\text{lim}}$ is significantly larger than the additional term due to friction. For this reason, in Case 1 the effect of friction is negligible. [Chavarrías et al. \(2019a\)](#) studied Equation ((6.15)) and found that it can be both positive (i.e. the model is well-posed) or negative (i.e. the model is ill-posed). For this reason, in testing for ill-posedness of the system of equations we must test that it is well-posed for both wave numbers tending to infinity.

In Case 2, the maximum imaginary part of the two eigenvalues is equal to 0. For this reason, this case does not limit well-posedness of the model. Worded differently, in testing well-posedness of the model it is not necessary to study the case in which $k_{wx} = 0$ and $k_{wy} \rightarrow \text{inf}$.

In Case 3, the expression of the maximum imaginary part of the eigenvalues is too complicated to analyze. However, numerical tests show that that it can be positive. Worded differently, this direction needs to be tested.

6.3 Effect of Modifying the Time Scale of Mixing Processes in the 2D Model

In this section we analytically study the effect of modifying the time scale of mixing processes. We compute the characteristic polynomial of matrix \mathbf{M} (Equation (5.17)). The characteristic polynomial has complex coefficients and is of second order. We solve the polynomial equation and compute the limit as both wave numbers (i.e., in the x and y direction) tend to infinity (i.e., short wave perturbations). Finally, we study the imaginary component of the resulting solution.

The regularization parameter α multiplies the whole imaginary part of the eigenvalues as the wave number tends to infinity (the details of the analysis will be included in a future appendix). For this reason, parameter α changes the absolute value of the growth rate of perturbations but not the sign. Worded differently, using parameter α one does not change whether perturbations grow or decay. We conclude the modification of the time scale of the mixing processes does not regularize the two-dimensional active layer model.

The details are found in Appendix B.

6.4 Effect of Adding Diffusion to the Active Layer Equation in the 2D Model

In this section we conduct the same analysis as the one performed in Section 6.3 here considering the effect of the regularization strategy consisting of including diffusion in the active layer equation. We find the following results. First, a certain amount of diffusion in the stream-wise direction (i.e., $\kappa_{Hx} \neq 0$) always regularizes a situation that is ill-posed if diffusion is not taken into consideration. The minimum amount of diffusion necessary to regularize the model can be computed analytically for a simplified case (i.e., two sediment size fractions assuming quasi-steady flow). The diffusion coefficient in the transverse direction (κ_{Hy}) has no effect in regularizing the model. The details are found in Appendix C.

We present an example of the effect of diffusion. To this end, we consider Case H2 (Tables 5.1 and 5.3). This case is ill-posed when no diffusion is taken under consideration (Figure 6.1a). When diffusion is equal to $-5 \text{ m}^2/\text{s}$ the same conditions yield a well-posed model (Figure 6.1c).

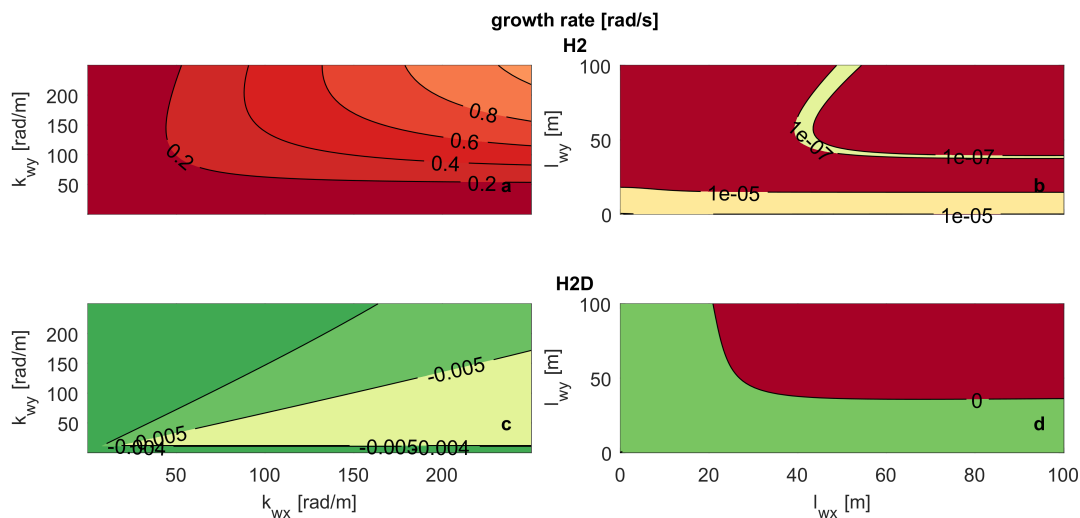


Figure 6.1: Growth rate of perturbations added to the reference case (tables 5.1 and 5.3) as a function of the wave number and the wavelength: (a)-(b) $\kappa_{Hx} = 0$, (Case H2, ill-posed), (c)-(d) $\kappa_{Hx} = -5 \text{ m}^2/\text{s}$, (Case H2D, well-posed). The subplots in the two columns show the same information but highlight the behaviour for large wave numbers (left column) and for large wavelengths (right column). Red and green indicates growth and decay of perturbations, respectively.

Ideally, the regularization technique that we propose here also regularizes the one-dimensional. This would mean that we have one single regularization strategy for the active layer model independently on whether the model is one-dimensional or two-dimensional. Interestingly, preliminary results show that diffusion does not regularize the one-dimensional system of equations.

7 Implementation

In this section we first describe the previous implementation of the routines to identify conditions in which the active layer model is ill-posedness in Delft3D-4 (Section 7.1). This allows us to identify caveats and limitations. In Section 7.2 we describe the new implementation of the routines to check for ill-posedness. In Section 7.3 we describe the implementation of the regularization strategy.

7.1 Existing Routines

In this section we sketch the existing routines to identify ill-posed conditions in Delft3D-4. The implementation is done on a branch (https://svn.oss.deltares.nl/repos/delft3d/branches/research/Technical%20University%20of%20Delft/20161020_ellipticity_check) created from the trunk of Delft3D-4 at revision 6118 (20 October 2016 13:17:24).

The output of the implemented routines is a new output variable named `checkval` that indicates whether the model is, at the node under consideration, well-posed (`checkval=0`) or ill-posed (`checkval=1`). The check is conducted every time a map-type output is saved. The property is computed at the cell centers.

To compute this new variable, the function `trisol` is modified. After the flow computation of the second half time step, the test of the mathematical character of the model is conducted. The variables of the new routines are allocated (function `hirano_check_init`). Subsequently, the function `erosed` is called in a loop once for each dependent variable. In each call to `erosed`, one dependent variable is perturbed and the sediment transport rate for each size fractions is computed. For instance, when the flow discharge in the x direction is perturbed, we compute $q_{bk}(q_x + dq_x)$. A last call to the function yields the unperturbed sediment transport rate for each size fractions.

The function `trisol` continues normally until function `bott3d`. This function is modified to obtain as output the volume fraction content of sediment at the interface between the active layer and the substrate. After calling `bott3d`, function `trisol` calls a new function `hirano_check`. This new function yields as output the variable `checkval`.

In `hirano_check`, the matrices \mathbf{A}_x and \mathbf{A}_y are built. Then, the eigenvalues of each matrix are computed using the routine `rg` from EISPACK. If at least one of the eigenvalues of one of the matrices has an imaginary component different than 0, the variable `checkval` is set to 1. Otherwise, it is equal to 0.

As we only check the eigenvalues of matrices \mathbf{A}_x and \mathbf{A}_y , we are neglecting the effect of the diffusive component due to the bed slope effect, as well as the effect of friction. At this moment, but not when it was implemented, we are aware of the limitations of this implementation.

The derivatives are computed numerically. This is beneficial, as it allows for checking the mathematical character of the model for all closure relations for the sediment transport rate and hiding functions. However, this is done at the expenses of looping on `erosed`.

The routines check the mathematical character only before a map-type output is saved. Ideally, the mathematical character should be checked for each time step.

Finally, the routines are implemented in Delft3D-4 (curvilinear), while the future is Delft3D-FM.

This may not be a strong limitation, as the functions could be easily adapted to the Delft3D-FM.

7.2 Implementation of the new Detection Routines

In this section we describe the new implementation of the routines to detect ill-posedness. The implementation is done on a branch (https://svn.oss.deltares.nl/repos/delft3d/branches/research/TechnicalUniversityofDelft/20190405_Hirano_regularisation) created from the trunk of Delft3D-FM at revision 63587 (5 April 2019 07:36:30).

In avoiding the loop in morphology to numerically compute the necessary sediment transport derivatives, we have implemented two routines that compute the derivatives. These routines are called when calling routine `fm_eroded`, in which morphodynamic update is computed. This is the most reasonable location, as the sediment transport parameters are readily available. The derivatives can be computed either analytically or numerically by calling `sedtrans_analytical_derivatives` or `sedtrans_numerical_derivatives`, respectively. When computing analytically, the expressions in Appendix A are evaluated. Finite differences are used to compute the derivatives numerically. The benefit of the analytical expressions is that it is more accurate and it is expected to be faster, as less calls are needed than when computing the derivatives numerically. This computational time will largely depend on the number of size fractions. For the cases we have tested with up to three size fraction, we have not observed any significant time difference between the two methods. The drawback of the analytical expressions is that it is currently implemented for *Ashida and Michiue (1971)* only. The benefit of the numerical computation of the derivatives is that is available for all closure relations (assuming they are of the form describe in Section 2.2).

Once the derivatives are computed, a new function `fm_hirano_illposed_check` that provides as output whether the model is ill-posed, is called in routine `step_reduce`. In this new function matrix \mathbf{M} is built. Contrary to the previous implementation, this matrix depends on the wave number. Ill-posedness is defined for infinitely short waves. We select an arbitrary default short wavelength equal to 0.01 m (the value is set as input). By checking the eigenvalues for: (1) $k_{wx} = \frac{2\pi}{0.01}$ and $k_{wy} = 0$, and (2) $k_{wx} = k_{wy} = \frac{2\pi}{0.01}$ we are certain than the behaviour for short wave lengths is captured. It is not necessary to test the conditions for $k_{wx} = 0$ and $k_{wy} = \frac{2\pi}{0.01}$ as we have proven analytically that, in this case, for infinitely short waves the imaginary part of the eigenvalues is negative or equal to zero.

7.3 Implementation of the Regularization Strategy

In this section we describe the implementation of the regularization strategy consisting in adding diffusion to the active layer equation (Section 6.4). This is done in the same branch as the new routines to check for ill-posedness (Section 7.2).

After the conditions at each cell are tested and we know the cells in which the model is ill-posed, we compute the cells in which the regularization strategy will be applied. One option is that the regularization strategy is applied only at the cells in which the model is ill-posed. This, however, may yield an unstable solution. This is because, in an ill-posed case, a short wave pattern of aggradational and degradation follows from a short wave pattern of infinitesimal perturbations in bed elevation. Considering a case that is only ill-posed under degradational conditions (as it usually happens), the pattern of ill-posed cells also presents short wave perturbations. As a consequence, the regularization strategy is applied in a discontinuous manner. This is physically unrealistic, as the strategy is derived to account for the effect of mixing waves with a length scale several times the flow depth. For this reason, we have implemented the option that all cells at a certain distance from an ill-posed cell are regularized. The distance is user-specified.

In solving the regularized active layer equation (Equation (3.2)), we split it into the diffusive component and the advective component. We label as advective component the original part of the equation. To solve for the diffusive component, we treat the volume fraction content as a constituent and use the solver in routine `transport` by setting the source, sink, and advective velocity equal to zero. The diffusive component is added to the advective one when updating the bed stratigraphy in routine `bed_composition_module`.

The diffusion coefficient is at this moment user-specified. It is possible to numerically compute the minimum amount of diffusion that guarantees that the model is ill-posed. This is, however, expensive numerically. One consequence is that diffusion is the same everywhere in the domain.

8 Results

In this section we present the results. We test the implementation of the diffusive flux (Section 8.1) and apply the regularization to a laboratory experiment (Section 8.2) and a field case (Section 8.3).

8.1 Diffusion Test

In testing the implementation of the regularized active layer equation solver, we consider an idealized rectangular domain without flow. The initial condition is a flat bed with uniform grain size distribution consisting of Fraction 1 only. The grain size distribution of a rectangle situated in the centre of the domain is composed of Fraction 2 only (Figure 8.1). The diffusion coefficient is set to $-1 \times 10^{-2} \text{ m}^2/\text{s}$. The grain size distribution after 5 s is shown in Figure 8.2.

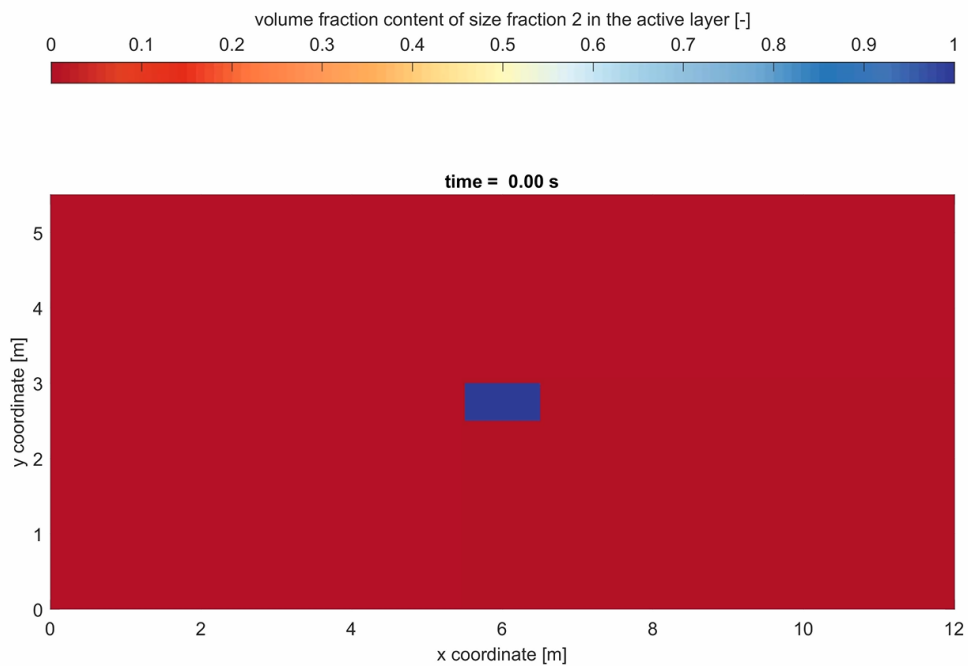


Figure 8.1: Initial condition of the numerical run to test the implementation of the regularized active layer solver.

To test whether the order of magnitude of the estimated diffusion is realistic, we compare the results with the analytical solution of a Dirac delta placed at the centre of the domain with coordinates (x_0, y_0) :

$$F_a = \frac{A}{4\pi t \sqrt{\kappa_x \kappa_y}} \exp\left(-\frac{(x-x_0)^2}{4\kappa_x t} - \frac{(y-y_0)^2}{4\kappa_y t}\right). \quad (8.1)$$

The analytical solution after 5 s is shown in Figure 8.3.

The order of magnitude of diffusion is the same. Note that the initial condition is different and for this reason it is not possible to exactly compare the solutions. It is not possible to impose

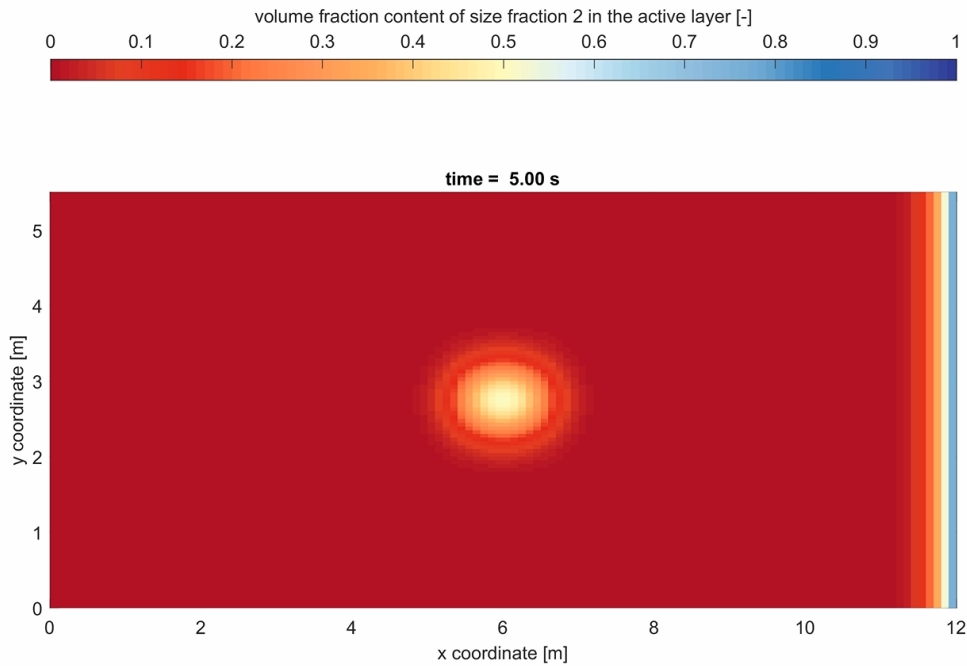


Figure 8.2: Condition after 5 s of the numerical run to test the implementation of the regularized active layer solver.

a Dirac delta as initial condition in the numerical simulation. Note also that for very small times, the analytical volume fraction content is larger than 1, which cannot be handled by the numerical solver.

In the numerical solution, there are changes at the right domain edge. This is because this domain is open and no boundary condition is prescribed. The initial condition of the ghost node propagates inside the domain. This effect occurs because we are applying the regularization strategy at all nodes (i.e., including ghost nodes) to force diffusion in the whole domain. When the regularization strategy is applied only at the cells in which the model is ill-posed, this effect will not be present.

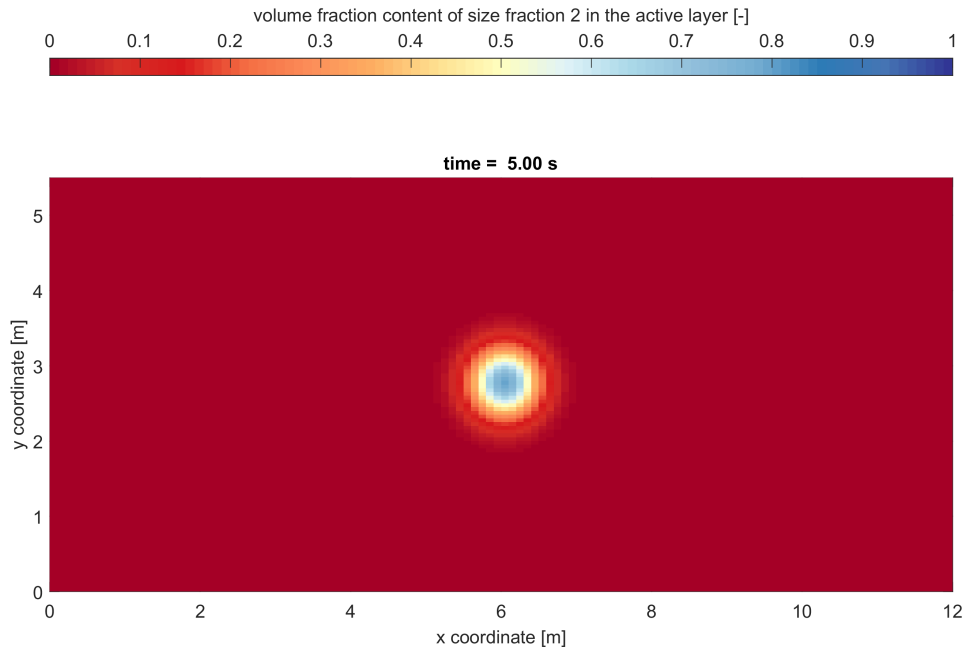


Figure 8.3: Condition after 5 s of the analytical solution.

8.2 Flume Experiment

In this section we apply the regularization strategy to a case inspired in the laboratory experiments conducted under condition in which the active layer model is ill-posed (*Chavarrías et al., 2019b*). The domain is 10 m long and 1 m wide. The grain size distribution is composed of two sediment size fraction with characteristic grain sizes equal to 2.108×10^{-3} m and 5.496×10^{-3} m. The upstream water discharge is equal to $0.15 \text{ m}^2/\text{s}$. The initial bed slope is equal to 2.7×10^{-3} . The friction coefficient is equal to 0.0104. The initial water depth is 0.204 m, which is under normal flow conditions. The downstream water level is lowered at a rate equal to 8 cm in 8 h. The upstream bed level is lowered at the same rate. The active layer thickness is equal to 1 cm. The substrate is composed of coarse sediment but for a patch between $x = 1 \text{ m}$ and $x = 9 \text{ m}$ along the whole width and 2 cm below the bed surface. The patch is composed of fine sediment only. The sediment transport rate is computed using the closure relation by *Ashida and Michiue (1971)*.

In Simulation 1, we do not apply the regularization strategy and we use a coarse grid discretiation ($\Delta x = 0.25 \text{ m}$, $\Delta y = 0.20 \text{ m}$). Figure 8.4 shows the bed elevation and mean grain size after 2.02 h. The routine predicts that the situation is ill-posed and a large physically unrealistic wave develops.

Simulation 2 is equal to Simulation 1 but for the fact that we use a finer grid ($\Delta x = \Delta y = 0.05 \text{ m}$). The physically unrealistic oscillation is larger, as we expect from an ill-posed simulation.

Simulation 3 is equal to Simulation 1 but for the fact that we apply the regularization strategy. This is applied at the cells which are predicted to be ill-posed only. The diffusion coefficient is

equal to $-0.15 \text{ m}^2/\text{s}$, which is the minimum amount to regularize this case. We observe that there are no large oscillations, but we observe small perturbations.

Simulation 4 is equal to Simulation 3 but for the fact that we apply the regularization strategy at all cells which at less than 0.5 m from a cell that is detected as ill-posed. This distance is based on the length scale of the mixing waves observed in the laboratory experiments. In this case, the simulation remains stable.

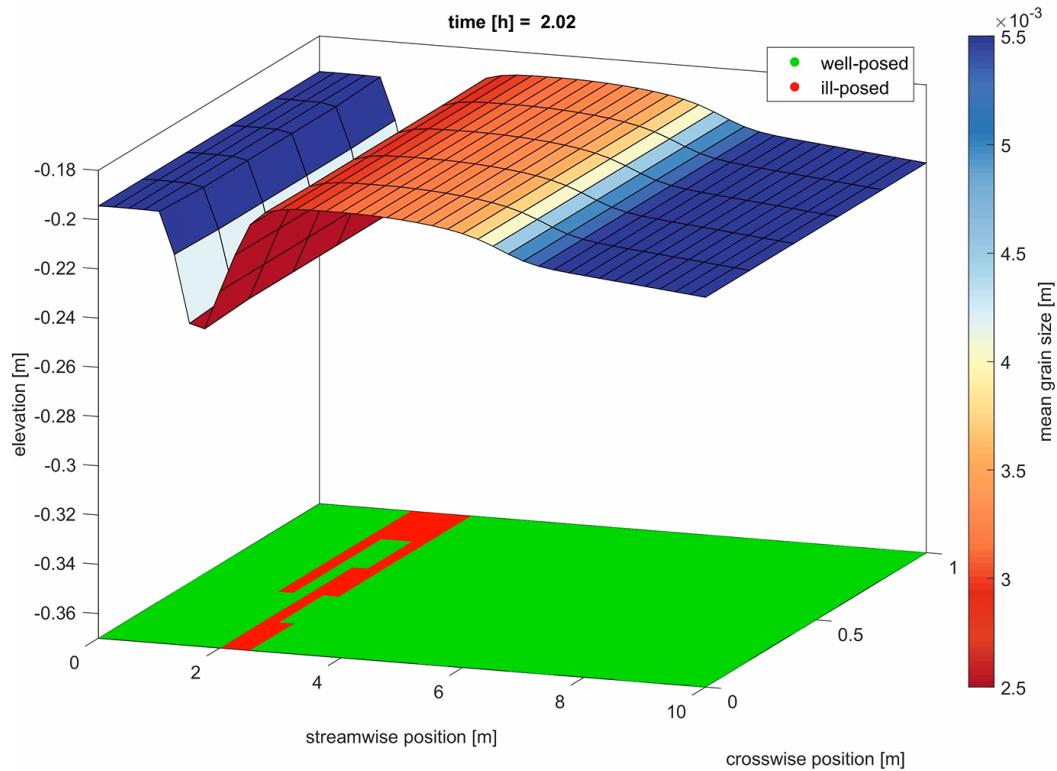


Figure 8.4: Bed elevation and mean grain size at the bed surface in Simulation 1 (ill-posed, not regularized, and coarse grid).

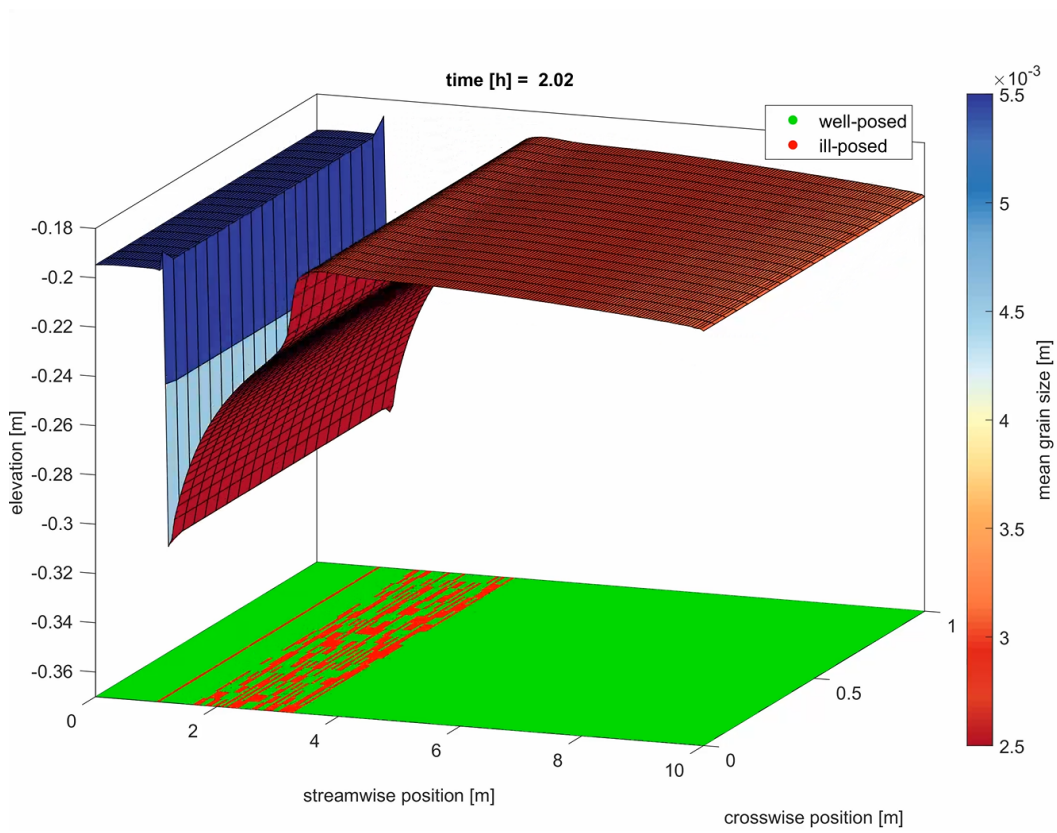


Figure 8.5: Bed elevation and mean grain size at the bed surface in Simulation 2 (ill-posed, not regularized, and fine grid).

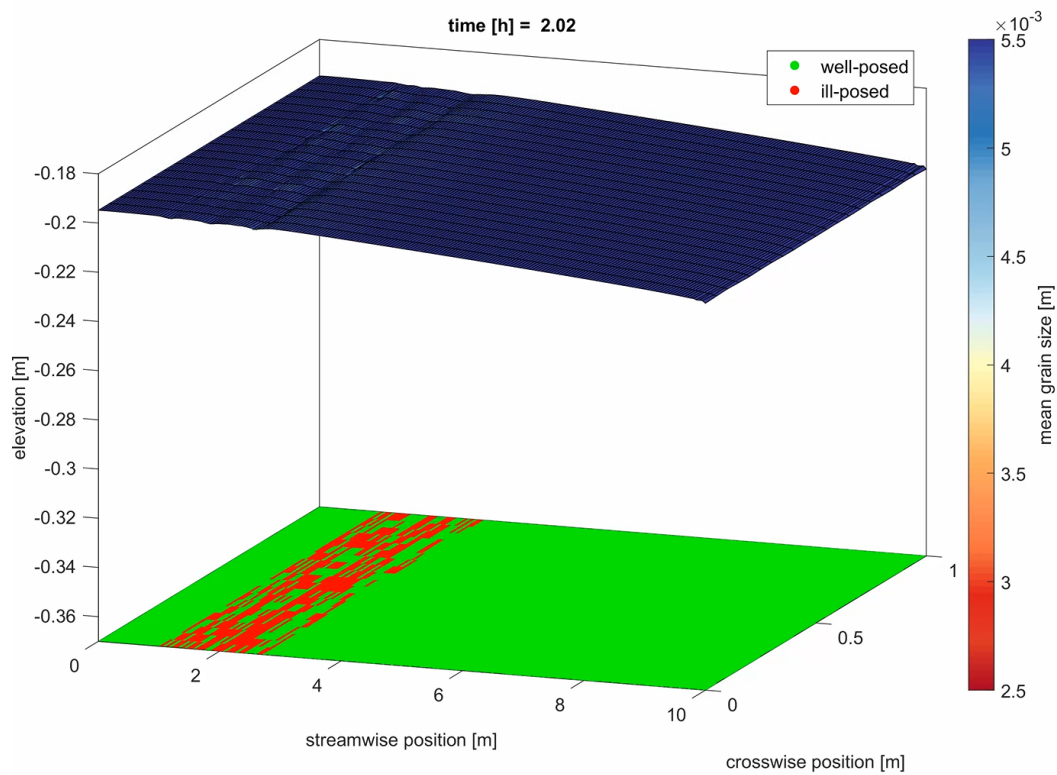


Figure 8.6: Bed elevation and mean grain size at the bed surface in Simulation 3 (ill-posed, regularized only at ill-posed cells, and fine grid). The green (red) red colour in the $x - y$ plane indicate the locations that would be well-posed (ill-posed) if the model would have not been regularized.

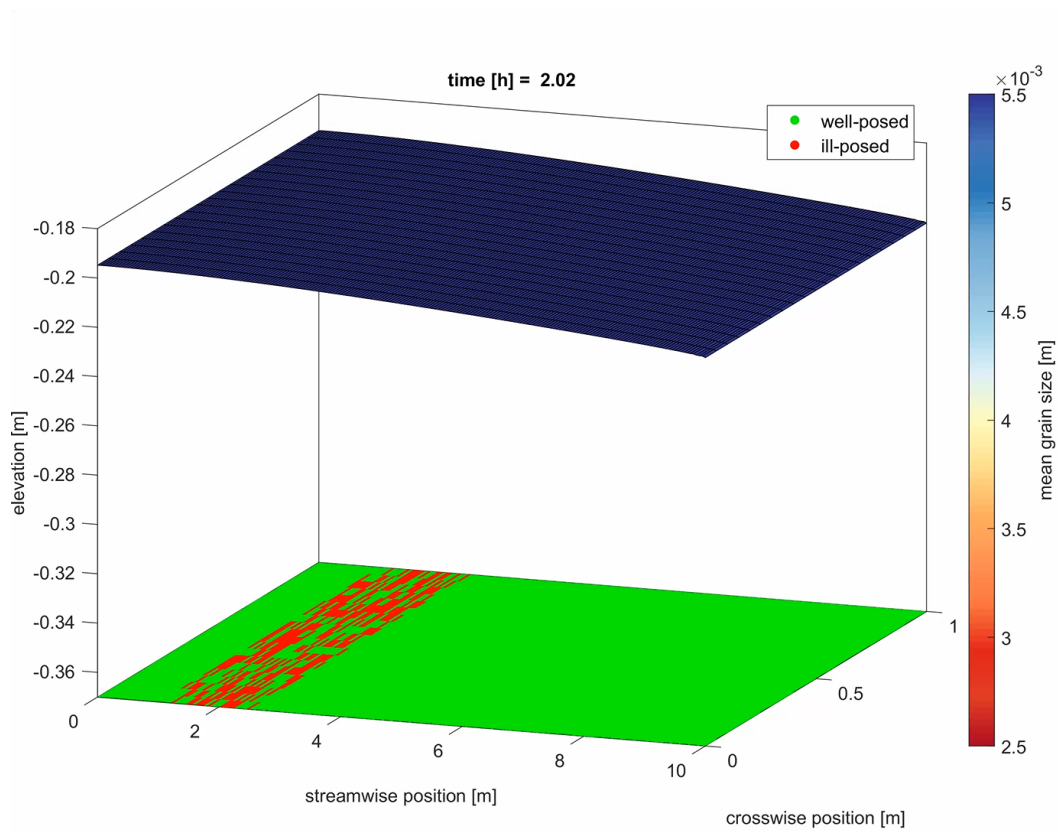


Figure 8.7: Bed elevation and mean grain size at the bed surface in Simulation 4 (ill-posed, regularized at cells within a radius, and fine grid). The green (red) red colour in the $x - y$ plane indicate the locations that would be well-posed (ill-posed) if the model would have not been regularized.

8.3 Field Application

In this section we apply the regularization strategy to a field application. We consider the schematization of the bifurcation area around Pannerdensch (simulation `delft3d_4-rijn-2017-v1`). We have converted this simulation from Delft3D-4 to Delft3D-FM. The original model runs a set of alternating constant discharges by using the SMT (Yossef *et al.*, 2008). This feature is not implemented in Delft3D-FM. We consider one single discharge equal to $2250 \text{ m}^3/\text{s}$. In an initial run, we obtain steady flow conditions for this discharge. This state is subsequently used as initial condition. We run for 1 h of morphodynamic update after 1 h of spin-up. Testing whether the Delft3D-FM simulation provides similar results as the Delft3D-4 one is outside the scope of this project. Figure 8.8 shows a view of the grid.

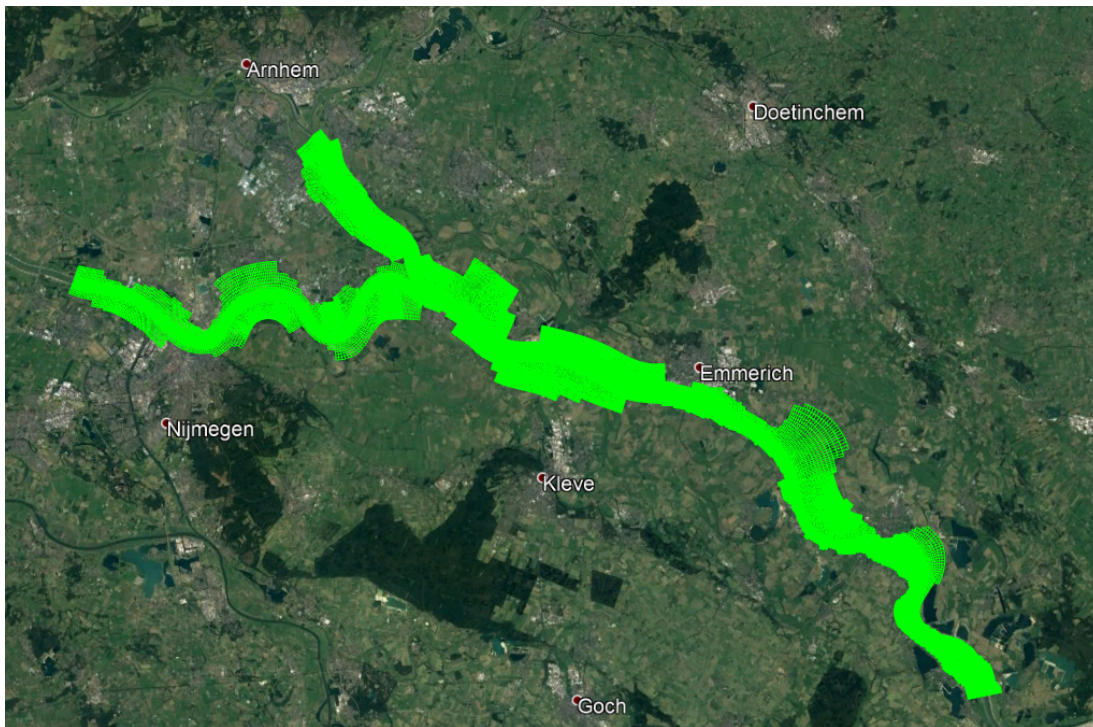


Figure 8.8: Computational domain.

We run a simulation without applying the regularization strategy and a simulation regularizing all the cells at less than 150 m from an ill-posed node using a diffusion coefficient equal to $-3 \text{ m}^2/\text{s}$. The distance guarantees that the regularization strategy is applied at sufficiently large regions rather than at individual cells. The diffusion coefficient is a conservative estimate based on characteristic conditions. However, we cannot guarantee that this value is enough to regularize all conditions in the domain. We observed unrealistic patterns in the regularized simulation. We noted that not all cells had an initial grain size distribution below the first top layer. While the current implementation in Delft3D-FM of the active layer model can deal with such cases, it is unclear what the regularized model does. It is important to note that, for instance, ill-posedness depends on the grain size distribution at the interface between the active layer and the substrate. In the original schematization, the active layer thickness is a function of the flow depth. In principle, the regularization strategy can be applied in cases with variable active layer thickness. This option, however, has not been tested and has not been considered in the analytical study.

For these reasons, we consider a modified grain size distribution in which there is always sediment underneath the active layer. Arbitrarily, we set a layer of practically infinite thickness composed of sediment between 0.001 m and 0.002 m. We also set the active layer thickness

to a constant value equal to 1 m.

Figure 8.10 shows the cumulative erosion or sedimentation after 1 h of morphodynamic update for the case in which the regularization strategy is not applied. We focus on a 6 km region of the Boven-Rijn (Figure 8.9). Figure 8.10 shows the locations in which the active layer model is predicted to be ill-posed. We observe large aggradation and degradation (up to 1 cm) in neighbouring cells at the locations in which the model is ill-posed. It is important to note that in Figure 8.10 we show the locations in which the model is ill-posed at a certain time. It can (and has) been ill-posed at other locations before. However, as the simulation time is short, it is a good approximation of the overall condition. A pattern of large aggradation and degradation in neighbouring cells is the expected consequence of ill-posedness.

In Figure 8.12 we show the results of applying the regularization strategy. We observe that the pattern of large aggradation and degradation at the right bank has decreased substantially, which is the expected consequence of regularizing an ill-posed case. We also note large aggradation in particular cells, especially in the left side of the river. We do not think that this pattern is physically realistic. We think that this unexpected result may be due to the fact that we have not considered the interaction between the regularization technique and other elements of this schematization such as fixed layers. For instance, the current implementation diffuses sediment on top of groynes, which is not physically realistic. We also note that in the current implementation diffusion is not restricted to active cells. This means that changes in the grain size distribution diffuse from ill-posed location in the main channel to the floodplain.

The explicit time solver of Delft3D-FM imposes restrictive time steps when considering diffusion processes in which the Péclet number is large (i.e., when diffusion is large relative to advection). This time restriction is overcome by limiting the time step based on advection processes only. As a consequence, the diffusion computed by the model is smaller than intended. This may have consequences if the necessary diffusion to regularize the active layer model is large compared to the advection. This cases would not be regularized regardless of the prescribed diffusion coefficient. It may be possible that in the current simulations diffusion computed by the model is smaller than intended and it is actually ill-posed.

Overall, we consider this exercise as a preliminary test. We do not think that the current implementation is ready for a complex field scenario given the fact that we have considered a simplified case in deriving and testing the regularization strategy.

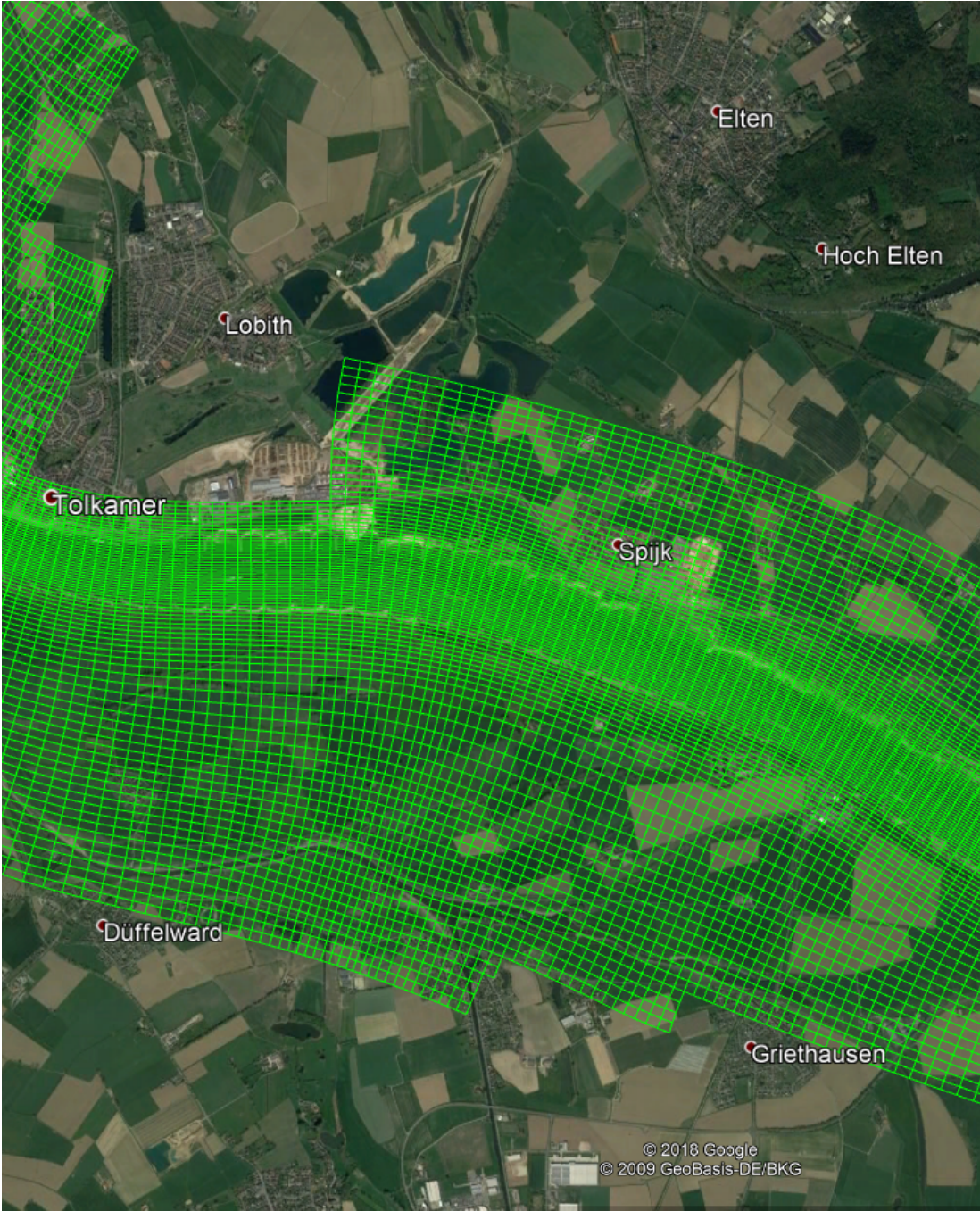


Figure 8.9: Area of interest.

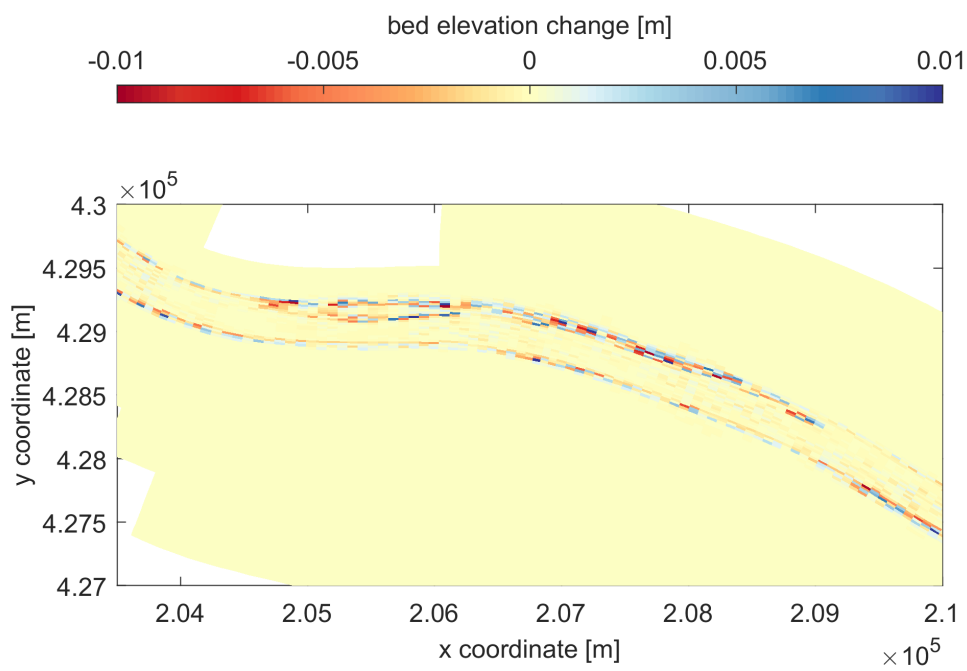


Figure 8.10: Bifurcation simulation without regularization strategy.

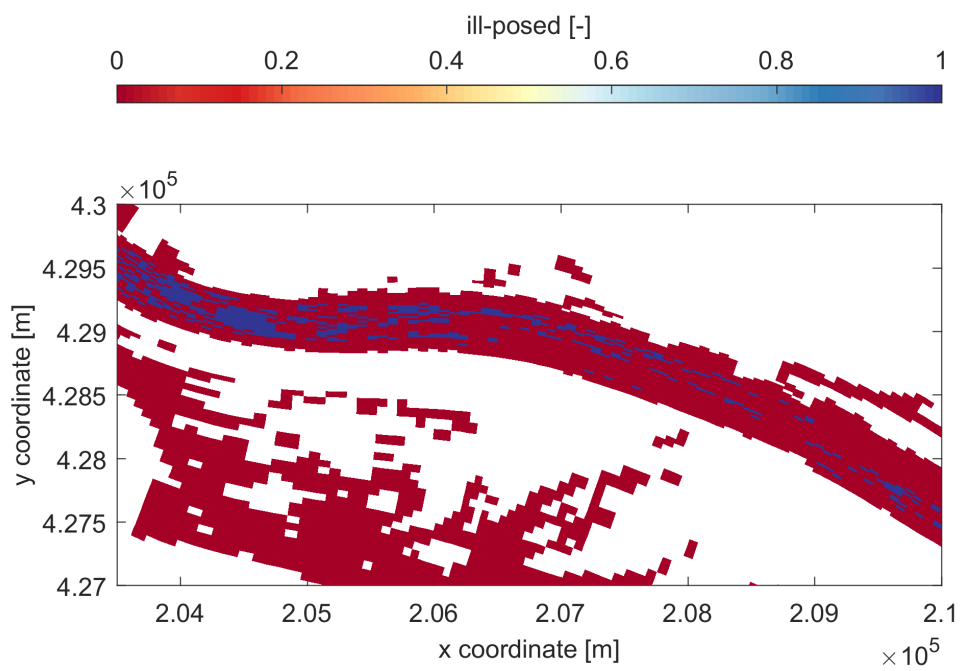


Figure 8.11: Ill-posedness domain.

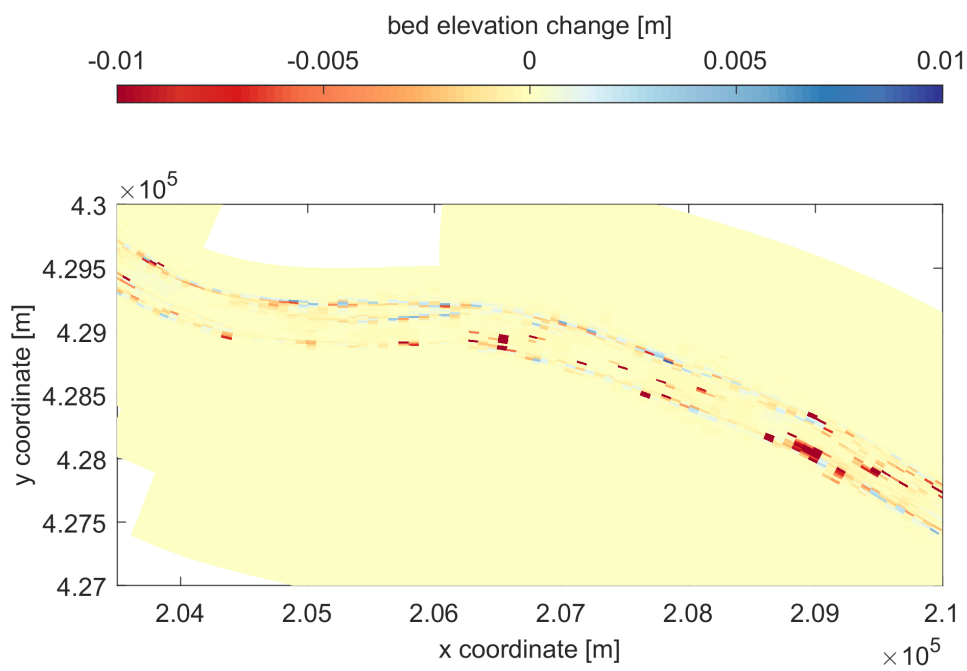


Figure 8.12: Bifurcation simulation with regularization strategy.

9 Recommendations

In this section we discuss the following steps to make the regularization strategy general and applicable at field cases.

The theoretical analysis should be extended to consider the case of a variable active layer thickness and the interaction with fixed layers. We have assumed that the friction coefficient is independent on the flow depth and grain size. We do not expect that the domain of ill-posedness significantly depends on this assumption. This is because the simplifications inherent to the active layer and sediment transport models appear to us significantly cruder than the simplification of the friction coefficient. However, including this effect would strengthen and generalize the analysis. In order to include it, one would need to linearise the friction equation to obtain its change with time. The system of equations would be composed of one more equation, which would increase the difficulty of analytical findings.

Further testing is required as regards to the routines for testing for ill-posedness. We have tested that the matrices are correct with only up to 3 size fractions, none of which is tracer sediment. In principle, the methodology should be able to deal with tracer sediment, but maybe matrices become ill-conditioned under some circumstances, as the sediment transport capacity of two size fractions in the mixture is the same when dealing with tracer sediment. We have tested the matrices when sediment transport occurs in one direction only. Further testing is required to verify that the grid orientation does not play a role. We have verified that the matrices are correctly built and the eigenvalues are correct when using the sediment transport relation by *Ashida and Michiue (1971)*. This has been done computing the derivatives both analytically and numerically. Further testing is required to verify that no unexpected implementation problems arise when using different sediment transport relations.

It is important to prevent diffusion in non-active cells. Similarly, there is a need to implement a mechanism to deal with structures such as groynes. A routine to estimate diffusion is also important to make the tool applicable to general cases. Currently, the same amount of diffusion is applied at all regularized cells. Ideally, the amount of diffusion would be computed for each case independently (i.e., spatially varying diffusion).

The implementation of the regularization strategy needs to be further tested. Similar exercises as the one conducted in Section 8.1 need to be done including, at least, more size fractions, tracer sediment, structures, variable active layer thickness, and fixed layers.

Updating the bed using the right amount of diffusion is crucial to regularize the system of equations. In the current trunk version of Delft3D-FM, it is possible to limit the time step such that the right amount of diffusion is used in the computation. However, this was developed after the research branch was created. For this reason, it is uncertain whether the correct amount of diffusion is used. Overall, the research branch needs to be merged with the trunk. Otherwise, we cannot benefit from further development and fixes of the trunk.

10 Conclusions

The model that accounts for mixed-size sediment in morphodynamic processes (i.e., the active layer model) may be ill-posed under certain circumstances. When the model is ill-posed it loses its predictive capabilities, as it is unstable to short wave perturbations and the solution does not converge when the numerical grid is refined. *Chavarrías et al. (2019b)* devised a regularization strategy to guarantee that the model is unconditionally well-posed. The strategy was tested under one dimensional conditions only. In this document we show that the extension to two dimensions of the strategy devised by *Chavarrías et al. (2019b)* does not regularize the two-dimensional version of the active layer model.

We propose a different regularization strategy and we prove that it yields an unconditionally well-posed model. This second strategy is based on adding a diffusive flux to the active layer equation which accounts for mixing processes occurring at a small scale not resolved by the model.

We implement a routine to test for ill-posedness in Delft3D-FM. This routine considers the effect of the bed slope on the sediment transport direction, contrary to the previous implementation. Moreover, we expect the computation to be faster.

We implement and test the regularization strategy. We use it to regularize a model representing the a laboratory experiment conducted under conditions in which the active layer model is ill-posed. The results are satisfactory. While the non-regularized simulation presents physically unrealistic oscillations, the regularized simulation remains stable.

Finally, we convert a Delft3D-4 schematization of the bifurcation area around Pannerden to Delft3D-FM and run two simulations to test the effect of the regularization strategy on a field scenario. The non-regularized run presents a pattern of aggradation and degradation compatible with ill-posedness. The regularized run decreases this pattern. However, aggradation occurs in unexpected areas. This is most probably related to interaction of the regularization strategy with other functionalities such as fixed layers, and structures. Further development is required for the regularization strategy to be applicable in general.

A Sediment Transport Closure Relations and its Derivatives

In this section we write the necessary derivatives to compute matrix \mathbf{M} (Equation ((5.17))) for the closure relations described in Section 2.2. In Section A.2 we describe the closure relations for accounting for the hiding effect. In Section A.3 we describe the closure relations to compute the mean grain size.

A.1 Nondimensional Sediment Transport

In this section we describe the closure relations and the derivatives to compute the nondimensional sediment transport rate.

A.1.1 *Ashida and Michiue* (1971) Nondimensional Sediment Transport

The closure relation for the nondimensional sediment transport rate predicted by *Ashida and Michiue* (1971) is:

$$q_{bk}^* = A (\theta_k - \xi_k \theta_c) \left(\sqrt{\theta_k} - \sqrt{\xi_k \theta_c} \right) \quad \forall k, \quad (\text{A.1})$$

where $A = 17 [-]$ is a nondimensional coefficient and $\theta_c = 0.05 [-]$ is the nondimensional critical shear stress.

The derivative with respect to the nondimensional bed shear stress is:

$$\frac{\partial q_{bk}^*}{\partial \theta_k} = A \left[\frac{(\theta_k - \xi_k \theta_c)}{2\sqrt{\theta_k}} + \left(\sqrt{\theta_k} - \sqrt{\xi_k \theta_c} \right) \right] \quad \forall k. \quad (\text{A.2})$$

The derivative with respect to the hiding function is:

$$\frac{\partial q_{bk}^*}{\partial \xi_k} = \frac{-A\theta_c}{2} \left[\frac{(\theta_k - 3\xi_k \theta_c)}{\sqrt{\xi_k \theta_c}} + 2\sqrt{\theta_k} \right] \quad \forall k. \quad (\text{A.3})$$

A.1.2 *Engelund and Hansen* (1967) Nondimensional Sediment Transport

The fractional form (*Blom et al., 2016, 2017*) of the relation proposed by *Engelund and Hansen* (1967) neglecting form drag reads:

$$q_{bk}^* = \frac{A}{C_f} \theta_k^{5/2} \quad \forall k, \quad (\text{A.4})$$

where $A = 0.05 [-]$ is a nondimensional coefficient.

The derivative with respect to the nondimensional bed shear stress is:

$$\frac{\partial q_{bk}^*}{\partial \theta_k} = \frac{5}{2} \frac{A}{C_f} \theta_k^{3/2} \quad \forall k. \quad (\text{A.5})$$

The derivative with respect to the hiding function is:

$$\frac{\partial q_{bk}^*}{\partial \xi_k} = 0 \quad \forall k. \quad (\text{A.6})$$

A.2 Hiding Relations

In this section we describe the closure relations and the derivatives to account for the hiding effect.

A.2.1 *Ashida and Michiue (1971)* Hiding Relation

The hiding relation by *Ashida and Michiue (1971)* reads:

$$\xi_k = \begin{cases} 0.8429 \left(\frac{d_k}{D_m} \right)^{-1} & \text{for } \frac{d_k}{D_m} \leq 0.38889 \\ \left(\frac{\log_{10}(19)}{\log_{10}(19 \frac{d_k}{D_m})} \right)^2 & \text{for } \frac{d_k}{D_m} > 0.38889 \end{cases} \quad \forall k . \quad (\text{A.7})$$

The derivative with respect to the mean grain size is:

$$\frac{\partial \xi_k}{\partial D_m} = \begin{cases} \frac{0.8429}{d_k} & \text{for } \frac{d_k}{D_m} \leq 0.38889 \\ \frac{2(\log_{10}(19) \ln(10))^2}{D_m \left[\ln\left(\frac{19d_k}{D_m}\right) \right]^3} & \text{for } \frac{d_k}{D_m} > 0.38889 \end{cases} \quad \forall k . \quad (\text{A.8})$$

A.3 Mean Grain Size

In this section we describe the closure relations and the derivatives to compute mean grain size.

A.3.1 Arithmetic Mean Grain Size

The arithmetic mean grain size is:

$$D_m = \sum_{k=1}^N F_{ak} d_k = d_N + \sum_{k=1}^{N-1} F_{ak} (d_k - d_N) . \quad (\text{A.9})$$

The expression on the right hand side of Equation ((A.9)) accounts for the constrain in Equation ((2.12)).

The derivative with respect to the volume fraction content of sediment in the active layer is:

$$\frac{\partial D_m}{\partial F_{al}} = d_l - d_N \quad l \in [1, N - 1] . \quad (\text{A.10})$$

A.3.2 Geometric Mean Grain Size

The geometric mean grain size is:

$$D_m = d_{\text{ref}} 2^{-\phi_m} , \quad (\text{A.11})$$

where ϕ_m [–] denotes the geometric mean grain size in ϕ -scale:

$$\phi_m = \sum_{k=1}^N \phi_k F_{ak} , \quad (\text{A.12})$$

where ϕ_k denotes the grain size k in ϕ -scale:

$$\phi_k = -\log_2 \left(\frac{d_k}{d_{\text{ref}}} \right) . \quad (\text{A.13})$$

Parameter d_{ref} [m] denotes a reference grain size (e.g. $d_{\text{ref}} = 1 \text{ mm}$) to obtain the right dimensions.

In terms of the dependent variables of the model and accounting for the constrain in Equation ((2.12)), the geometric mean grain size is:

$$D_m = d_{\text{ref}} 2^{\log_2\left(\frac{d_N}{d_{\text{ref}}}\right) + \sum_{k=1}^{N-1} F_{ak} \log_2\left(\frac{d_k}{d_N}\right)}, \quad (\text{A.14})$$

The derivative with respect to the volume fraction content of sediment in the active layer is:

$$\frac{\partial D_m}{\partial F_{al}} = d_N \ln(2) \log_2\left(\frac{d_l}{d_N}\right) \prod_{k=1}^{N-1} \left(\frac{d_k}{d_N}\right)^{F_{ak}} \quad l \in [1, N-1]. \quad (\text{A.15})$$

B Proof that a Modification of the Time Scale of Mixing does not Regularize the 2D Model

In this section we prove that a modification of the time scale of the mixing processes does not regularize the active layer model under two-dimensional conditions. To this end, we consider a case with two sediment size fractions.

In order to study well-posedness of the model, *Chavarrías et al. (2019a)* computed the maximum imaginary part of the eigenvalues assuming quasi-steady flow as the wave number $k_{wx} = k_{wy} \rightarrow \text{inf}$. The eigenvalues ω are the solution of the second order characteristic polynomial:

$$\mathbf{R} = \begin{bmatrix} 0 & 0 & 0 & 0 & 0 \\ 0 & 0 & 0 & 0 & 0 \\ 0 & 0 & 0 & 0 & 0 \\ 0 & 0 & 0 & \omega & 0 \\ 0 & 0 & 0 & 0 & \omega \end{bmatrix} - \mathbf{M}_0 \quad . \quad (\text{B.1})$$

We rewrite their expression as:

The modification of the time scale of the mixing processes is done by using a preconditioning matrix \mathbf{P} such that the linear model is *Chavarrías et al. (2019b)*:

$$\mathbf{P} \frac{\partial \mathbf{Q}'}{\partial t} + \mathbf{D}_{x0} \frac{\partial^2 \mathbf{Q}'}{\partial x^2} + \mathbf{D}_y \frac{\partial^2 \mathbf{Q}'}{\partial y^2} + \mathbf{C}_0 \frac{\partial^2 \mathbf{Q}'}{\partial x \partial y} + \mathbf{A}_{x0} \frac{\partial \mathbf{Q}'}{\partial x} + \mathbf{A}_{y0} \frac{\partial \mathbf{Q}'}{\partial y} + \mathbf{B}_0 \mathbf{Q}' = 0, \quad (\text{B.2})$$

where the preconditioning matrix \mathbf{P} is:

$$\mathbf{P} = \begin{bmatrix} 1 & 0 & 0 & 0 & 0 \\ 0 & 1 & 0 & 0 & 0 \\ 0 & 0 & 1 & 0 & 0 \\ 0 & 0 & 0 & 1 & 0 \\ 0 & 0 & 0 & 0 & \alpha_p \end{bmatrix} \quad , \quad (\text{B.3})$$

where $\alpha_p > 1$ is a preconditioning factor. The complete matrix of the linear model is in this case:

$$\mathbf{M}_0 = \mathbf{P}^{-1} \mathbf{D}_{x0} k_{wx}^2 \mathbf{i} + \mathbf{P}^{-1} \mathbf{D}_{y0} k_{wy}^2 \mathbf{i} + \mathbf{P}^{-1} \mathbf{A}_{x0} k_{wx} + \mathbf{P}^{-1} \mathbf{A}_{y0} k_{wy} - \mathbf{P}^{-1} \mathbf{B}_0 \mathbf{i} \quad . \quad (\text{B.4})$$

We notice that the effect of the preconditioning technique is to divide the last row of matrix \mathbf{M}_0 by α_p . For this reason, we can easily assess the effect of the preconditioning technique by considering that variables γ_{x1} , γ_{y1} , l_{y1} , and $\mu_{y1,1}$ of the non-preconditioned system turn into $\gamma_{x1p} = \gamma_{x1}/\alpha_p$, $\gamma_{y1p} = \gamma_{y1}/\alpha_p$, $l_{y1p} = l_{y1}/\alpha_p$, and $\mu_{y1,1p} = \mu_{y1,1}/\alpha_p$ in the preconditioned system, respectively.

We substitute the preconditioned variables in the original eigenvalues to write the maximum growth rate of the preconditioned system as a function of the variables of the non-preconditioned one:

$$\omega_{i_p}^{\text{lim}} = \frac{1}{\alpha_p^2} \left[\omega_i^{\text{lim}} + \frac{u^2 \chi_{x1}}{R_y} (1 - \alpha_p) (r_{y1} - c_{x1}) e_x^{\text{lim}} \right] \quad . \quad (\text{B.5})$$

Under conditions in which the active layer model is ill-posed, $\omega_i^{\text{lim}} > 0$. Given that $\frac{u^2 \chi_{x1}}{R_y} < 0$, $(1 - \alpha_p) < 0$, $e_x^{\text{lim}} > 0$, and $(r_{y1} - c_{x1})$ can be positive, we conclude that there are cases in which the modification of the time scale of the mixing processes does not regularize the system of equations.

A particular case that cannot be regularized is the one in which the sediment transport rate is computed using the relation by *Engelund and Hansen (1967)* and the bed slope effect does not account for the effect of the bed shear stress. Under these conditions:

$$r_{y1} = c_{x1} = \frac{q_{b1}}{q_b} . \quad (\text{B.6})$$

In this case it is clear that the sign of ω_{ip}^{lim} is equal to the sign of ω_i^{lim} regardless of the value of α_p . Moreover, in this particular case, $r_{y1} = c_{y1}$ such that:

$$\omega_{ip}^{\text{lim}} = \frac{-u^2 \chi_{x1}^2}{R_y} l_{y1} (r_{y1} - d_{x1,1}) . \quad (\text{B.7})$$

As in this case $r_{y1} > d_{x1,1}$, the sign of l_{y1} determines whether the model is well-posed or ill-posed.

C Proof that Diffusion in Hirano Regularizes the 2D Model

In this section we prove that diffusion in the active layer equation regularizes the active layer model considering two sediment size fractions. The matrices in this case are the same as in the ones presented in Appendix B but for the terms (5,5) in matrices \mathbf{D}_{x0} and \mathbf{D}_{y0} which are equal to $-\kappa_{Hx}$ and $-\kappa_{Hy}$, respectively. We compute the eigenvalues as the solution of a second order characteristic polynomial. In guaranteeing well-posedness, we study the behavior for large wave numbers. We consider three cases:

- 1 $k_{wx} = k_{wy} \rightarrow \inf$
- 2 $k_{wx} = 0$ and $k_{wy} \rightarrow \inf$
- 3 $k_{wx} \rightarrow \inf$ and $k_{wy} = 0$

Note that in proving that a modification of the time scales does not regularize the system, it is sufficient to prove that in one of these cases the regularization strategy is unsuccessful. However, in proving that diffusion always regularizes the system of equations, it is necessary to prove that for the three cases the maximum imaginary part of the eigenvalues is negative.

In Case 1, the maximum imaginary part of the eigenvalues is equal to:

$$\omega_i^{\lim} = \begin{cases} \frac{k_{wx}(1-Fr)^2 + k_{wy}}{2-Fr^2} (-\kappa_{Hx} - \kappa_{Hy}) & \text{for } -\kappa_{Hx} - \kappa_{Hy} - R_y \geq 0 \\ \frac{k_{wx}(1-Fr)^2 + k_{wy}}{2-Fr^2} R_y & \text{for } -\kappa_{Hx} - \kappa_{Hy} - R_y < 0 \end{cases} \quad (C.1)$$

We see that the growth rate is negative regardless of the value of the diffusion coefficients. Thus, Case 1 does not limit well-posedness of the model.

In Case 2, the maximum imaginary part of the eigenvalues is equal to:

$$\omega_i^{\lim} = \begin{cases} k_{wy}^2 R_y & \text{for } \kappa_{Hy} + R_y \geq 0 \\ -k_{wy}^2 \kappa_{Hy} & \text{for } \kappa_{Hy} + R_y < 0 \end{cases} \quad (C.2)$$

We see that the growth rate is negative regardless of the value of the diffusion coefficients. Thus, Case 2 does not limit well-posedness of the model.

In Case 3, the maximum imaginary part of the eigenvalues is equal to:

$$\omega_i^{\lim} = \frac{-\psi_x^* C_f g}{u} \omega_i^{\lim*}, \quad (C.3)$$

where:

$$\omega_i^{\lim*} = \begin{cases} \frac{\chi_{x1} \gamma_{x1}}{\kappa_{Hx}^*} - Fr^* & \text{for } \Delta_\omega \leq 0 \\ \frac{\chi_{x1} \gamma_{x1}}{\kappa_{Hx}^*} - Fr^* \frac{\psi^* + \Delta_\omega}{\psi^*} - \frac{Fr^2 \Delta_\omega}{\psi^*} & \text{for } \Delta_\omega > 0 \end{cases}, \quad (C.4)$$

where $\kappa_{Hx}^* < 0$ [-] denotes a nondimensional diffusion coefficient:

$$\kappa_{Hx}^* = \frac{-\kappa_{Hx} C_f g}{u^3}, \quad (C.5)$$

parameter $\psi_x^* > 0$ [-] denotes a Froude-dependent value ψ_x :

$$\psi_x^* = \frac{\psi_x}{1 - Fr^2}, \quad (C.6)$$

parameter $\text{Fr}^* < 0$ [–] denotes a function of the Froude number:

$$\text{Fr}^* = \frac{3\text{Fr}^4}{\text{Fr}^2 - 1}, \quad (\text{C.7})$$

and parameter Δ_ω [–] denotes a discriminant between the two branches of the solution:

$$\Delta_\omega = -(\text{Fr}^* + \text{Fr}^2) \kappa_{\text{Hx}}^* - \psi_x^* + \chi_{x1} \mu_{x1,1}. \quad (\text{C.8})$$

In Case 3 there is a minimum amount of diffusion in the x direction necessary to guarantee that the growth rate is negative. As diffusion tends to 0, the sign of the growth rate depends on γ_{x1} , which is consistent with the analysis based on the one-dimensional model by [Stecca et al. \(2014\)](#) and [Chavarrías et al. \(2018\)](#).

For the case that $\Delta_\omega > 0$, the minimum amount of diffusion can be computed implicitly only. However, we can compute the diffusion coefficient explicitly for the case $\Delta_\omega < 0$:

$$\kappa_{\text{Hx}_{\min}} = \frac{u^3 \chi_{x1} \gamma_{x1}}{C_f g \text{Fr}^*}. \quad (\text{C.9})$$

References

- Armanini, A., and G. di Silvio (1988), A one-dimensional model for the transport of a sediment mixture in non-equilibrium conditions, *J. Hydraul. Res.*, 26(3), 275–292, doi:10.1080/00221688809499212.
- Ashida, K., and M. Michiue (1971), An investigation of river bed degradation downstream of a dam, in *Proc. of the 14th IAHR World Congress, 29 August–3 Septemeber, Paris, France*, vol. 3, pp. 247–255.
- Baar, A. W., J. de Smit, W. S. J. Uijttewaal, and M. G. Kleinhans (2018), Sediment transport of fine sand to fine gravel on transverse bed slopes in rotating annular flume experiments, *Water Resour. Res.*, 54(1), 19–45, doi:10.1002/2017WR020604.
- Balmforth, N. J., and S. Mandre (2004), Dynamics of roll waves, *J. Fluid Mech.*, 514, 1–33, doi:10.1017/S0022112004009930.
- Balmforth, N. J., and A. Vakil (2012), Cyclic steps and roll waves in shallow water flow over an erodible bed, *J. Fluid Mech.*, 695, 35–62, doi:10.1017/jfm.2011.555.
- Banks, J., J. Brooks, G. Cairns, G. Davis, and P. Stacey (1992), On Devaney's definition of chaos, *The American Mathematical Monthly*, 99(4), 332–334, doi:10.2307/2324899.
- Barker, B., M. A. Johnson, P. Noble, L. M. Rodrigues, and K. Zumbrun (2017a), Note on the stability of viscous roll waves, *C. R. Mec.*, 345(2), 125–129, doi:10.1016/j.crme.2016.11.001.
- Barker, B., M. A. Johnson, P. Noble, L. M. Rodrigues, and K. Zumbrun (2017b), Stability of viscous St. Venant roll waves: From onset to infinite Froude number limit, *J. Nonlinear Sci.*, 27(1), 285–342, doi:10.1007/s00332-016-9333-6.
- Barker, T., and J. M. N. T. Gray (2017), Partial regularisation of the incompressible μ -rheology for granular flow, *J. Fluid Mech.*, 828, 5–32, doi:10.1017/jfm.2017.428.
- Barker, T., D. G. Schaeffer, P. Bohorquez, and J. M. N. T. Gray (2015), Well-posed and ill-posed behaviour of the μ -rheology for granular flow, *J. Fluid Mech.*, 779, 794–818, doi:10.1017/jfm.2015.412.
- Begnudelli, L., A. Valiani, and B. F. Sanders (2010), A balanced treatment of secondary currents, turbulence and dispersion in a depth-integrated hydrodynamic and bed deformation model for channel bends, *Adv. Water Resour.*, 33(1), 17–33, doi:10.1016/j.advwatres.2009.10.004.
- Bell, R. G., and A. J. Sutherland (1983), Nonequilibrium bedload transport by steady flows, *J. Hydraul. Eng.*, 109(3), 351–367, doi:10.1061/(ASCE)0733-9429(1983)109:3(351).
- van Bendegom, L. (1947), Eenige beschouwingen over riviermorphofogie en rivierverbetering, *De Ingenieur*, 59(4), 1–11, (in Dutch).
- Bennett, J. P., and C. F. Nordin (1977), Simulation of sediment transport and armouring, *Hydrol. Sci. Bull.*, 22(4), 555–569, doi:10.1080/02626667709491760.
- Blom, A. (2008), Different approaches to handling vertical and streamwise sorting in modeling river morphodynamics, *Water Resour. Res.*, 44(3), W03,415, doi:10.1029/2006WR005474.
- Blom, A., E. Viparelli, and V. Chavarrías (2016), The graded alluvial river: Profile concavity and downstream fining, *Geophys. Res. Lett.*, 43(12), 6285–6293, doi:10.1002/2016GL068898.

- Blom, A., L. Arkesteijn, V. Chavarrías, and E. Viparelli (2017), The equilibrium alluvial river under variable flow and its channel-forming discharge, *J. Geophys. Res., Earth Surface*, 122(10), 1924–1948, doi:10.1002/2017JF004213.
- Bressan, A. (2011), Hyperbolic conservation laws, in *Mathematics of Complexity and Dynamical Systems*, edited by R. A. Meyers, chap. 44, pp. 729–739, Springer, New York, NY, United States, doi:10.1007/978-1-4614-1806-1_44.
- Callander, R. A. (1969), Instability and river channels, *J. Fluid Mech.*, 36, 465–480, doi:10.1017/S0022112069001765.
- Cao, Z., and P. A. Carling (2002), Mathematical modelling of alluvial rivers: Reality and myth. Part 1: General review, *Proceedings of the Institution of Civil Engineers Water & Maritime Engineering*, 154(3), 207–219.
- Castro, M. J., E. D. Fernández-Nieto, A. M. Ferreiro, J. A. García-Rodríguez, and C. Parés (2009), High order extensions of Roe schemes for two-dimensional nonconservative hyperbolic systems, *J. Sci. Comput.*, 39(1), 67–114, doi:10.1007/s10915-008-9250-4.
- Chavarrías, V., G. Stecca, and A. Blom (2018), Ill-posedness in modelling mixed-sediment river morphodynamics, *Adv. Water Resour.*, 114, 219–235, doi:10.1016/j.advwatres.2018.02.011.
- Chavarrías, V., R. Schielen, W. Ottevanger, and A. Blom (2019a), Ill posedness in modelling two-dimensional morphodynamic problems: Effects of bed slope and secondary flow, *J. Fluid Mech.*, 868, 461–500, doi:10.1017/jfm.2019.166.
- Chavarrías, V., G. Stecca, A. Siviglia, and A. Blom (2019b), A regularization strategy for modeling mixed-sediment river morphodynamics, *Adv. Water Resour.*, 127, 291–309, doi:10.1016/j.advwatres.2019.04.001.
- Colombini, M., and A. Stocchino (2005), Coupling or decoupling bed and flow dynamics: Fast and slow sediment waves at high froude numbers, *Phys. Fluids*, 17(3), 036,602, doi:10.1063/1.1848731.
- Colombini, M., and A. Stocchino (2012), Three-dimensional river bed forms, *J. Fluid Mech.*, 695, 63–80, doi:10.1017/jfm.2011.556.
- Colombini, M., G. Seminara, and M. Tubino (1987), Finite-amplitude alternate bars, *J. Fluid Mech.*, 181, 213–232, doi:10.1017/S0022112087002064.
- Cordier, S., M. Le, and T. M. de Luna (2011), Bedload transport in shallow water models: Why splitting (may) fail, how hyperbolicity (can) help, *Adv. Water Resour.*, 34(8), 980–989, doi:10.1016/j.advwatres.2011.05.002.
- Courant, R., and D. Hilbert (1989), *Methods of Mathematical Physics, Volume 2: Differential Equations*, 852 pp., John Wiley & Sons, New York, NY, United States.
- Dafermos, C. M. (2010), *Hyperbolic Conservation Laws in Continuum Physics*, no. 325 in *Grundlehren der mathematischen Wissenschaften*, 3 ed., 708 pp., Springer-Verlag Berlin-Heidelberg, Heidelberg, Germany.
- Dafermos, C. M. (2016), Introduction to the theory of hyperbolic conservation laws, in *Handbook of Numerical Methods for Hyperbolic Problems, Handbook of Numerical Analysis*, vol. 17, edited by R. Abgrall and C.-W. Shu, chap. 1, pp. 1–18, Elsevier, Amsterdam, the Netherlands, doi:10.1016/bs.hna.2016.08.003.

- Deigaard, R., and J. Fredsøe (1978), Longitudinal grain sorting by current in alluvial streams, *Nord. Hydrol.*, 9(1), 7–16, doi:10.2166/nh.1978.002.
- Devaney, R. L. (1989), *An Introduction to Chaotic Dynamical Systems*, 336 pp., Addison-Wesley, Boston, MA, United States.
- Einstein, H. A. (1950), The bed-load function for sediment transportation in open channel flows, *Tech. Bull. 1026*, US Department of Agriculture, Soil Conservation Service, Washington, DC, United States, 70 pp.
- Engelund, F., and E. Hansen (1967), Monograph on sediment transport in alluvial streams, *Tech. Rep.*, Hydraulics Laboratory, Technical University of Denmark, Copenhagen, Denmark, 63 pp.
- Engelund, F., and O. Skovgaard (1973), On the origin of meandering and braiding in alluvial streams, *J. Fluid Mech.*, 57(2), 289–302, doi:10.1017/S0022112073001163.
- Exner, F. M. (1920), Zur Physik der Dünen, *Akad. Wiss. Wien Math. Naturwiss.*, 129(2a), 929–952, (in German).
- Flokstra, C. (1977), The closure problem for depth-averaged 2-D flow, in *Proc. 18th IAHR World Congress, 15–19 August, Baden-Baden, Germany*, p. 580.
- Fowler, A. C. (1997), *Mathematical Models in the Applied Sciences*, Cambridge Texts in Applied Mathematics, 424 pp., Cambridge University Press, Cambridge, United Kingdom.
- Fredsøe, J. (1978), Meandering and braiding of rivers, *J. Fluid Mech.*, 84(4), 609–624, doi:10.1017/S0022112078000373.
- Garegnani, G., G. Rosatti, and L. Bonaventura (2011), Free surface flows over mobile bed: Mathematical analysis and numerical modeling of coupled and decoupled approaches, *Commun. Appl. Ind. Math.*, 2(1), e371, doi:10.1685/journal.caim.371.
- Garegnani, G., G. Rosatti, and L. Bonaventura (2013), On the range of validity of the Exner-based models for mobile-bed river flow simulations, *J. Hydraul. Res.*, 51(4), 380–391, doi:10.1080/00221686.2013.791647.
- Hadamard, J. S. (1923), *Lectures on Cauchy's problem in linear partial differential equations*, 316 pp., Yale University Press, New Haven, CT, United States.
- Hirano, M. (1971), River bed degradation with armoring, *Proc. Jpn. Soc. Civ. Eng.*, 195, 55–65, doi:10.2208/jscej1969.1971.195_55.
- Hoey, T. B., and R. I. Ferguson (1994), Numerical simulation of downstream fining by selective transport in gravel bed rivers: Model development and illustration, *Water Resour. Res.*, 30(7), 2251–2260, doi:10.1029/94WR00556.
- Ikeda, S., G. Parker, and K. Sawai (1981), Bend theory of river meanders. Part 1. Linear development, *J. Fluid Mech.*, 112, 363–377, doi:10.1017/S0022112081000451.
- Jagers, B. (2003), Modelling planform changes of braided rivers, Ph.D. thesis, University of Twente, Enschede, the Netherlands.
- Jain, S. C. (1992), Note on lag in bedload discharge, *J. Hydraul. Eng.*, 118(6), 904–917, doi:10.1061/(ASCE)0733-9429(1992)118:6(904).
- Jeffreys, H. (1925), The flow of water in an inclined channel of rectangular section, *The London, Edinburgh, and Dublin Philosophical Magazine and Journal of Science*, 49(293), 793–807, doi:10.1080/14786442508634662.

- Jop, P., Y. Forterre, and O. Pouliquen (2005), Crucial role of sidewalls in granular surface flows: Consequences for the rheology, *J. Fluid Mech.*, 541, 167–192, doi:10.1017/S0022112005005987.
- Jop, P., Y. Forterre, and O. Pouliquen (2006), A constitutive law for dense granular flows, *Nature*, 441, 727–730, doi:10.1038/nature04801.
- Joseph, D., and J. Saut (1990), Short-wave instabilities and ill-posed initial-value problems, *Theor. Comput. Fluid Mech.*, 1(4), 191–227, doi:10.1007/BF00418002.
- Kabanikhin, S. I. (2008), Definitions and examples of inverse and ill-posed problems, *J. Inv. Ill-Posed Problems*, 16, 317–357, doi:10.1515/JIIP.2008.019.
- Kalkwijk, J. P. T., and H. J. de Vriend (1980), Computation of the flow in shallow river bends, *J. Hydraul. Res.*, 18(4), 327–342, doi:10.1080/00221688009499539.
- Knowles, J. K., and E. Sternberg (1975), On the ellipticity of the equations of nonlinear elastostatics for a special material, *J. Elast.*, 5(3), 341–361, doi:10.1007/BF00126996.
- Knowles, J. K., and E. Sternberg (1976), On the failure of ellipticity of the equations for finite elastostatic plane strain, *Arch. Ration. Mech. Anal.*, 63(4), 321–336, doi:10.1007/BF00279991.
- Lax, P. D. (1980), On the notion of hyperbolicity, *Commun. Pure Appl. Math.*, 33(3), 395–397.
- Lee, H.-Y., and A. J. Odgaard (1986), Simulation of bed armoring in alluvial channels, *J. Hydraul. Eng.*, 112(9), 794–801, doi:10.1061/(ASCE)0733-9429(1986)112:9(794).
- Lesser, G., J. Roelvink, J. van Kester, and G. Stelling (2004), Development and validation of a three-dimensional morphological model, *Coastal Eng.*, 51(8–9), 883–915, doi:10.1016/j.coastaleng.2004.07.014.
- LeVeque, R. J. (2004), *Finite Volume Methods for Hyperbolic Problems*, no. 31 in Cambridge Texts in Applied Mathematics, Cambridge University Press, Cambridge, United Kingdom, doi:10.1017/CBO9780511791253.
- Lorenz, E. N. (1963), Deterministic nonperiodic flow, *J. Atmos. Sci.*, 20(2), 130–141, doi:10.1175/1520-0469(1963)020<0130:DNF>2.0.CO;2.
- Lyn, D. A., and M. Altinakar (2002), St. Venant-Exner equations for near-critical and transcritical flows, *J. Hydraul. Eng.*, 128(6), 579–587, doi:10.1061/(ASCE)0733-9429(2002)128:6(579).
- Meyer-Peter, E., and R. Müller (1948), Formulas for bed-load transport, in *Proc. 2nd IAHR World Congress, 6–9 June, Stockholm, Sweden*, pp. 39–64.
- Mosselman, E. (2005), Basic equations for sediment transport in CFD for fluvial morphodynamics, in *Computational Fluid Dynamics: Applications in Environmental Hydraulics*, edited by P. D. Bates, S. N. Lane, and R. I. Ferguson, chap. 4, pp. 71–89, John Wiley & Sons, Chichester, United Kingdom.
- Murray, A. B. (2007), Reducing model complexity for explanation and prediction, *Geomorphology*, 90(3–4), 178–191, doi:10.1016/j.geomorph.2006.10.020.
- Murray, A. B., and C. Paola (1994), A cellular model of braided rivers, *Nature*, 371(54), 54–57, doi:10.1038/371054a0.

- Murray, A. B., and C. Paola (1997), Properties of a cellular braided-stream model, *Earth Surf. Process. Landf.*, 22(11), 1001–1025, doi:10.1002/(SICI)1096-9837(199711)22:11<1001::AID-ESP798>3.0.CO;2-O.
- Paola, C. (2000), Quantitative models of sedimentary basin filling, *Sedimentology*, 47(s1), 121–178, doi:10.1046/j.1365-3091.2000.00006.x.
- Paola, C., and M. Leeder (2011), Environmental dynamics: Simplicity versus complexity, *Nature*, 469, 38–39, doi:10.1038/469038a.
- Paola, C., P. L. Heller, and C. L. Angevine (1992), The large-scale dynamics of grain-size variation in alluvial basins, 1: Theory, *Basin Res.*, 4(2), 73–90, doi:10.1111/j.1365-2117.1992.tb00145.x.
- Parker, G. (1991), Selective sorting and abrasion of river gravel. I: Theory, *J. Hydraul. Eng.*, 117(2), 131–147, doi:10.1061/(ASCE)0733-9429(1991)117:2(131).
- Parker, G., and E. D. Andrews (1985), Sorting of bed load sediment by flow in meander bends, *Water Resour. Res.*, 21(9), 1361–1373, doi:10.1029/WR021i009p01361.
- Parker, G., and A. J. Sutherland (1990), Fluvial armor, *J. Hydraul. Res.*, 28(5), 529–544, doi:10.1080/00221689009499044.
- Petts, G., M. Thoms, K. Brittan, and B. Atkin (1989), A freeze-coring technique applied to pollution by fine sediments in gravel-bed rivers, *Sci. Total Environ.*, 84, 259–272, doi:10.1016/0048-9697(89)90388-4.
- Phillips, B. C., and A. J. Sutherland (1989), Spatial lag effects in bed load sediment transport, *J. Hydraul. Res.*, 27(1), 115–133, doi:10.1080/00221688909499247.
- Rahuel, J., F. Holly, J. Chollet, P. Belleudy, and G. Yang (1989), Modeling of riverbed evolution for bedload sediment mixtures, *J. Hydraul. Eng.*, 115(11), 1521–1542, doi:10.1061/(ASCE)0733-9429(1989)115:11(1521).
- Ribberink, J. S. (1987), Mathematical modelling of one-dimensional morphological changes in rivers with non-uniform sediment, Ph.D. thesis, Delft University of Technology, Delft, the Netherlands.
- Rodrigues, L., and K. Zumbrun (2016), Periodic-coefficient damping estimates, and stability of large-amplitude roll waves in inclined thin film flow, *SIAM J. Math. Anal.*, 48(1), 268–280, doi:10.1137/15M1016242.
- Saint-Venant, A. J. C. B. (1871), Théorie du mouvement non permanent des eaux, avec application aux crues des rivières et à l'introduction des marées dans leur lit, *Comptes Rendus des séances de l'Académie des Sciences*, 73, 237–240, (in French).
- Schielen, R., A. Doelman, and H. E. de Swart (1993), On the nonlinear dynamics of free bars in straight channels, *J. Fluid Mech.*, 252, 325–356, doi:10.1017/S0022112093003787.
- Seminara, G. (2006), Meanders, *J. Fluid Mech.*, 554, 271–297, doi:10.1017/S0022112006008925.
- Shields, A. (1936), Anwendung der Ähnlichkeitsmechanik und Turbulenzforschung auf die Geschiebebewegung, Ph.D. thesis, Versuchsanstalt für Wasserbau und Schiffbau, 26, Berlin, Germany, (in German).
- Sieben, J. (1997), Modelling of hydraulics and morphology in mountain rivers, Ph.D. thesis, Delft University of Technology, Delft, the Netherlands.

- Siviglia, A., G. Stecca, and A. Blom (2017), Modeling of mixed-sediment morphodynamics in gravel bed rivers using the active layer approach: Insights from mathematical and numerical analysis, in *Gravel-Bed Rivers: Process and Disasters*, edited by D. Tsutsumi and J. Laronne, chap. 26, pp. 703–728, Wiley-Blackwell, Hoboken, NJ, United States, doi:10.1002/9781118971437.ch26.
- Stecca, G., A. Siviglia, and A. Blom (2014), Mathematical analysis of the Saint-Venant-Hirano model for mixed-sediment morphodynamics, *Water Resour. Res.*, 50(10), 7563–7589, doi:10.1002/2014WR015251.
- Strikwerda, J. (2004), *Finite Difference Schemes and Partial Differential Equations*, 2 ed., 427 pp., Society for Industrial and Applied Mathematics, Philadelphia, PA, United States, doi:10.1137/1.9780898717938.
- Toro, E. F. (2009), *Riemann Solvers and Numerical Methods for Fluid Dynamics*, 3 ed., 724 pp., Springer-Verlag Berlin-Heidelberg, Heidelberg, Germany, doi:10.1007/b79761.
- Toro-Escobar, C. M., C. Paola, and G. Parker (1996), Transfer function for the deposition of poorly sorted gravel in response to streambed aggradation, *J. Hydraul. Res.*, 34(1), 35–53, doi:10.1080/00221689609498763.
- Turkel, E. (1999), Preconditioning techniques in computational fluid dynamics, *Annu. Rev. Fluid Mech.*, 31(1), 385–416, doi:10.1146/annurev.fluid.31.1.385.
- Veprek, R. G., S. Steiger, and B. Witzigmann (2007), Ellipticity and the spurious solution problem of k-p envelope equations, *Phys. Rev. B*, 76, 165,320, doi:10.1103/PhysRevB.76.165320.
- Vreugdenhil, C. B. (1994), *Numerical Methods for Shallow-Water Flow*, 262 pp., Springer, Dordrecht, the Netherlands, doi:10.1007/978-94-015-8354-1.
- de Vriend, H. J. (1977), A mathematical model of steady flow in curved shallow channels, *J. Hydraul. Res.*, 15(1), 37–54, doi:10.1080/00221687709499748.
- de Vriend, H. J. (1981), Steady flow in shallow channel bends, Ph.D. thesis, Delft University of Technology, Delft, the Netherlands.
- de Vries, M. (1965), Considerations about non-steady bed load transport in open channels, *Tech. Rep. 36*, Delft Hydraulics Laboratory, Delft, the Netherlands, 10 pp.
- Wilcock, P. R., and J. C. Crowe (2003), Surface-based transport model for mixed-size sediment, *J. Hydraul. Eng.*, 129(2), 120–128, doi:10.1061/(ASCE)0733-9429(2003)129:2(120).
- Woodhouse, M. J., A. R. Thornton, C. G. Johnson, B. P. Kokelaar, and J. M. N. T. Gray (2012), Segregation-induced fingering instabilities in granular free-surface flows, *J. Fluid Mech.*, 709, 543–580, doi:10.1017/jfm.2012.348.
- Wu, W. (2007), *Computational River Dynamics*, 494 pp., Taylor & Francis, London, United Kingdom.
- Yossef, M. F., H. Jagers, S. van Vuren, and A. Sieben (2008), Innovative techniques in modelling large-scale river morphology, in *Proceedings of the 4th International Conference on Fluvial Hydraulics (River Flow)*, 3-5 September, Cesme, Izmir, Turkey, edited by M. Altınakar, M. A. Kokpınar, İsmail Aydın, Şevket Cokgor, and S. Kirgoz, Kubaba Congress Department and Travel Services, Ankara, Turkey.